A kidney-specific genetic control module in mice governs endocrine regulation of the cytochrome P450 gene *Cyp27b1* essential for vitamin D_3 activation

Received for publication, July 14, 2017, and in revised form, August 10, 2017 Published, Papers in Press, August 14, 2017, DOI 10.1074/jbc.M117.806901

Mark B. Meyer[‡1], Nancy A. Benkusky[‡], Martin Kaufmann[§], Seong Min Lee[‡], Melda Onal[‡], Glenville Jones[‡], and J. Wesley Pike[‡]

From the [‡]Department of Biochemistry, University of Wisconsin-Madison, Madison, Wisconsin 53706 and the [§]Department of Biomedical and Molecular Sciences, Queen's University Kingston, Kingston, Ontario K7L 3N6, Canada

Edited by Joel Gottesfeld

The vitamin D endocrine system regulates mineral homeostasis through its activities in the intestine, kidney, and bone. Terminal activation of vitamin D_3 to its hormonal form, 1α,25-dihydroxyvitamin D_3 (1,25$(OH)_2D_3$), occurs in the kidney via the cytochrome P450 enzyme CYP27B1. Despite its importance in vitamin D metabolism, the molecular mechanisms underlying the regulation of the gene for this enzyme, *Cyp27b1*, are unknown. Here, we identified a kidney-specific control module governed by a renal cell-specific chromatin structure located distal to *Cyp27b1* that mediates unique basal and parathyroid hormone (PTH)-, fibroblast growth factor 23 (FGF23)-, and 1,25$(OH)_2D_3$-mediated regulation of *Cyp27b1* expression. Selective genomic deletion of key components within this module in mice resulted in loss of either PTH induction or FGF23 and 1,25$(OH)_2D_3$ suppression of *Cyp27b1* gene expression; the former loss caused a debilitating skeletal phenotype, whereas the latter conferred a quasi-normal bone mineral phenotype through compensatory homeostatic mechanisms involving *Cyp24a1*. We found that *Cyp27b1* is also expressed at low levels in non-renal cells, in which transcription was modulated exclusively by inflammatory factors via a process that was unaffected by deletion of the kidney-specific module. These results reveal that differential regulation of *Cyp27b1* expression represents a mechanism whereby 1,25$(OH)_2D_3$ can fulfill separate functional roles, first in the kidney to control mineral homeostasis and second in extra-renal cells to regulate target genes linked to specific biological responses. Furthermore, we conclude that these mouse models open new avenues for the study of vitamin D metabolism and its involvement in therapeutic strategies for human health and disease.

The vitamin D endocrine system serves to regulate mineral homeostasis through its actions in the intestine, kidney, and bone (1). Vitamin D_3 itself is sequentially activated via two specific chemical modifications that occur first in the liver by CYP2R1 to 25$(OH)D_3$[2] and then in the kidney by CYP27B1 to 1α,25-dihydroxyvitamin D_3 (1,25$(OH)_2D_3$), the active hormonal form of the vitamin (2). Blood levels of 1,25$(OH)_2D_3$ are also determined by rates of catabolism that represent the primary function of CYP24A1 in the kidney (3). CYP27B1 is also expressed at low levels in many non-renal target cells (NRTCs), particularly those of skin and the immune system, where local production of 1,25$(OH)_2D_3$ has been suggested to preferentially influence the many pleiotropic, non-calcemic functions of 1,25$(OH)_2D_3$ (4, 5). Neither the mechanisms nor the overall biological impact of these non-renal cellular sources of 1,25$(OH)_2D_3$ are clear, particularly in the context of circulating 1,25$(OH)_2D_3$, which is believed to be derived exclusively from the kidney. Despite these uncertainties, the regulated expression of *Cyp27b1* and *Cyp24a1* is well-recognized as central to the overall biological activity of the vitamin D endocrine system.

Cyp27b1 expression is known to be controlled in the kidney by many different factors. PTH represents the primary inducer (6, 7), whereas both 1,25$(OH)_2D_3$ (8) and FGF23 (9, 10) represent the major negative regulators of *Cyp27b1* expression. Indeed, the ability of PTH, FGF23, and 1,25$(OH)_2D_3$ to modulate the expression of *Cyp27b1* in the kidney comprises a key element of regulatory signaling that links adaptive vitamin D metabolism to the maintenance of mineral homeostasis. Interestingly, renal expression of *Cyp24a1* is reciprocally regulated by these same hormones; PTH suppresses and both 1,25$(OH)_2D_3$ and FGF23 induce *Cyp24a1* (11–14). This regulatory paradigm in the kidney highlights the critical importance

This work was supported by the Department of Biochemistry, University of Wisconsin-Madison, and University of Wisconsin Carbone Cancer Center Support Grant P30 CA014520 from the National Institutes of Health. The authors declare that they have no conflicts of interest with the contents of this article. The content is solely the responsibility of the authors and does not necessarily represent the official views of the National Institutes of Health.

This article was selected as one of our Editors' Picks.

[1] To whom correspondence should be addressed: Dept. of Biochemistry, University of Wisconsin-Madison, Hector F. DeLuca Biochemistry Laboratories, Rm. 543D, 433 Babcock Dr., Madison, WI 53706. Tel.: 608-262-8230; Fax: 608-263-7609; E-mail: markmeyer@wisc.edu.

[2] The abbreviations used are: 25$(OH)D_3$, 25-hydroxyvitamin D_3; 1,25$(OH)_2D_3$, 1α,25-dihydroxyvitamin D_3; PTH, parathyroid hormone; qPCR, quantitative real-time PCR; NRTC, non-renal target cell; TPTG, thyroparathyroid gland; PTG, parathyroid gland; ANOVA, analysis of variance; CREB, cAMP-response element-binding protein; pCREB, phosphorylated CREB; VDR, vitamin D receptor; LOD, limit of detection; bw, body weight; BMD, bone mineral density; μCT, micro-computed tomography; ChIP-seq, ChIP-sequencing; DHS, DNase I hypersensitivity sequencing; KS-ERM, kidney-specific endocrine regulatory module; NRTC-RM, non-renal target cell regulatory module; pol, polymerase; MSC, mesenchymal stem cell; CTCF, CCCTC-binding factor.

of the coordinated control of both *Cyp27b1* and *Cyp24a1* expression by these endocrine hormones not only in the maintenance of circulating $1,25(OH)_2D_3$, but in the orchestration of normal mineral homeostasis as well.

Despite the central importance of these two genes in vitamin D metabolism, little is known of the molecular mechanisms that underpin *Cyp27b1* regulation in the kidney by PTH, FGF23, or $1,25(OH)_2D_3$ at the genomic level or of the adaptive relationship that occurs between this modulation and that of *Cyp24a1* expression. It has been shown that PTH action at *Cyp27b1* involves the PKA signaling pathway and likely the CREB transcription factor (15) and that $1,25(OH)_2D_3$ action involves the nuclear vitamin D receptor (VDR) (16). This contrasts with the actions of the more recently discovered phosphaturic hormone FGF23, where limited insight has been gained with regard to the identities of both the FGF receptor isoform(s) and the transcription factor(s) that are involved in *Cyp27b1* expression (17, 18). Importantly, research over the past decade using unbiased genomic techniques now points to the likelihood that genes such as *Cyp27b1* may be regulated via genomic control regions located distal to their transcriptional start sites, a principle that we have found relevant to the vitamin D system (19, 20). The absence of fundamental mechanistic insight relative to *Cyp27b1* regulation has impeded progress in fully understanding the vitamin D metabolic system, its role in orchestrating mineral homeostasis, and the pathological impact of alterations in this system that can occur in a wide variety of human maladies, including autoimmune diseases and cancer.

Herein, we focused our efforts on understanding the expression and regulation of *Cyp27b1* in the mouse. Our results identify a complex, multicomponent endocrine regulatory module specific to the kidney that is governed by a chromatin structure that is absent in NRTCs. This module regulates both the basal expression of *Cyp27b1* in the kidney as well as its differential modulation by PTH, FGF23, and $1,25(OH)_2D_3$, but it does not control the expression of *Cyp27b1* in NRTCs by inflammatory agents such as LPS. These results highlight the differential regulation of *Cyp27b1 in vivo* and provide a starting point for further delineation of the precise molecular and genomic mechanisms through which both renal and non-renal tissues control the expression of *Cyp27b1*, production of $1,25(OH)_2D_3$, and therefore its local and endocrine biology.

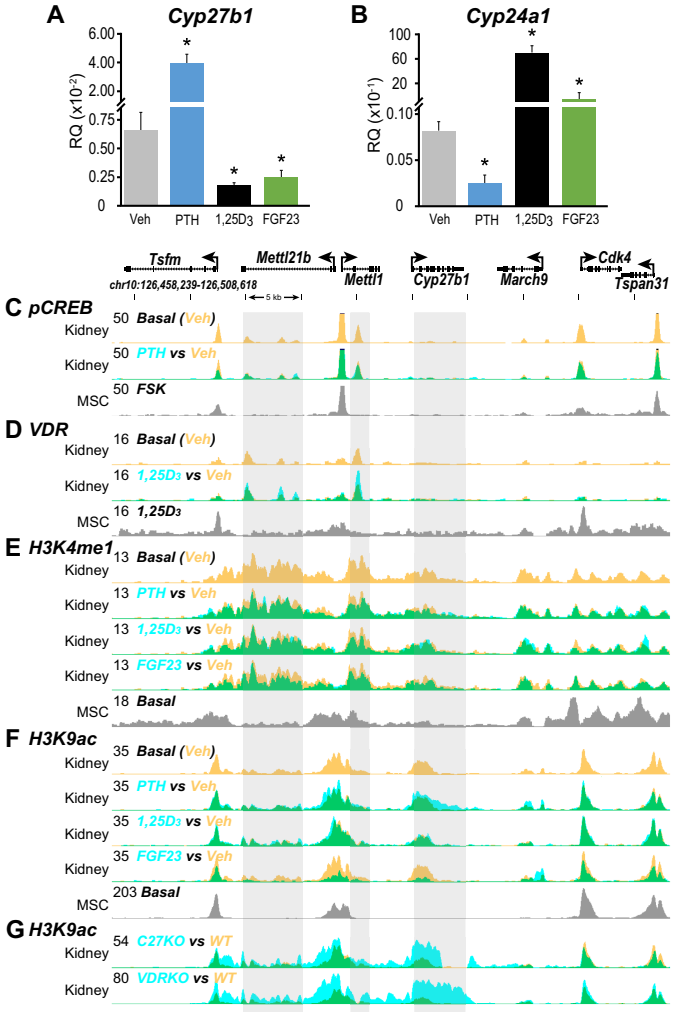

Figure 1. Cyp27b1 expression and genomic occupancy. Gene expression of *Cyp27b1* (*A*) and *Cyp24a1* (*B*) after treatment in 8–9-week-old C57BL/6 wild-type mice with ethanol/PBS vehicle (*Veh*, *gray*, $n = 6$), 230 ng/g bw PTH for 1 h (*PTH*, *blue*, $n = 6$), 10 ng/g bw $1,25(OH)_2D_3$ (*1,25D₃*, *black*, $n = 6$) for 6 h, or 50 ng/g bw FGF23 for 3 h (*FGF23*, *green*, $n = 6$). Data are displayed as relative quantitation (*RQ*, mean ± S.E.) compared with *Gapdh*. *, $p < 0.05$ paired *t* test, treatment *versus* vehicle. Overlaid ChIP-seq data tracks for pCREB (*C*), VDR (*D*), H3K4me1 (*E*), and H3K9ac (*F*) from mouse kidney displayed as either basal or vehicle (*yellow*, $n = 3$) or treated (*blue*, $n = 3$) with PTH, $1,25(OH)_2D_3$, or FGF23 as indicated with concentrations used in *A* and with a treatment time of 1 h. *G*, H3K9ac data in Cyp27b1KO mice (C27KO, *blue*) or VDRKO (*blue*) *versus* wild-type (*WT*, *yellow*). Overlapping track data appear as *green*. Regions of interest are highlighted in *light gray boxes*. Genomic location and scale are indicated (*top*), and maximum height of tag sequence density for each data track is indicated on the *y* axis (*top left each track*, normalized to input and 10^7 tags). Gene transcriptional direction is indicated by an *arrow* and exons by *boxes*.

Results

VDR and pCREB are bound upstream of the Cyp27b1 gene in a kidney-specific manner

Dose- and time-optimized i.p. injections for an acute maximal gene expression response by PTH, FGF23, and $1,25(OH)_2D_3$ into wild-type C57BL/6 (WT) mice lead to a dramatic up-regulation of *Cyp27b1* transcripts in the kidney in response to PTH and a significant suppression in response to both FGF23 and $1,25(OH)_2D_3$ (Fig. 1*A*). *Cyp24a1* expression in the kidney, in contrast, is reciprocally suppressed by PTH and induced by both FGF23 and $1,25(OH)_2D_3$ (Fig. 1*B*). Based upon this regulatory paradigm and the absence of insight into transcriptional activities, we utilized ChIP-seq analysis of the mouse kidney to identify the sites of action of both PTH and $1,25(OH)_2D_3$ at the *Cyp27b1* gene locus (the FGF23-activated transcription factor(s) has yet to be identified). ChIP-seq analysis of pCREB and VDR in kidneys of WT mice 1 h after a single injection (a time point previously optimized for primary genomic effects (21)) of either vehicle or cognate hormone revealed the presence of pCREB and VDR bound to DNA at the *Cyp27b1* locus (Fig. 1, *C* and *D*). The former was pre-bound to DNA and generally unaffected by PTH, whereas DNA binding of the latter was largely reinforced upon $1,25(OH)_2D_3$ injection at a single overlapping site within an intron of the upstream *Mettl1* gene and at three sites spanning the large intron located

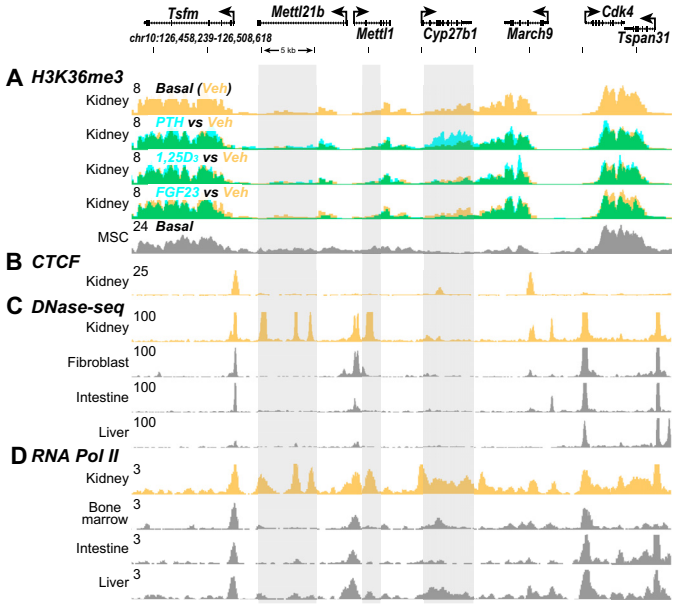

Figure 2. Transcriptional signatures modulated with treatment and steady-state ENCODE datasets confirm tissue specificity. *A,* H3K36me3 overlaid ChIP-seq data tracks displayed as vehicle (*yellow, n* = 3) or treated (*blue, n* = 3) with PTH (230 ng/g bw), 1,25(OH)$_2$D$_3$ (10 ng/g bw), or FGF23 (50 ng/g bw) as indicated with a treatment time of 1 h. Overlapping track data appear as *green*. ENCODE data tracks for CTCF (*B*), DNase hypersensitivity assay sequence (*DNase-seq*) (*C*), and RNA pol II ChIP-seq data (*D*) are displayed for kidney (*yellow*), fibroblast, intestine, liver, and bone marrow (*gray*). Regions of interest are highlighted in *light gray boxes*. Genomic location and scale are indicated (*top*), and maximum height of tag sequence density for each data track is indicated on the *y* axis (*top left each track,* normalized to input and 10^7 tags). Gene transcriptional direction is indicated by an *arrow* and exons by *boxes*.

in the *Mettl21b* gene (Fig. 1, *C* and *D*, highlighted by *gray vertical boxes*). Both genes produce methyltransferase-like proteins that are poorly characterized (22, 23). Neither pCREB nor VDR was observed immediately upstream of the *Cyp27b1* gene's transcriptional start site or in the introns of *Mettl1* or *Mettl21b* in marrow-derived mesenchymal stem cells (MSCs) (Fig. 1, *C* and *D*, *gray track*) following identical hormonal treatment. We also performed a ChIP-seq analysis of the transcription-confirming histone mark H3K36me3 1 h after injection (Fig. 2*A*). Modulation of H3K36me3 showed that each of these hormones, including FGF23, mediated direct regulation of the *Cyp27b1* gene body in the kidney. Equally important, these experimental results identified potential sites of regulatory action for at least two of the three primary mineral-regulating hormones at the *Cyp27b1* gene.

VDR and pCREB are localized to active enhancers in the introns of Mettl1 and Mettl21b

To determine whether the binding sites were localized to active enhancer regions (24), ChIP-seq analyses of the histone enhancer signature marks H3K4me1 and H3K9ac were performed in kidneys following a 1-h treatment of either vehicle or each of the three hormones (Fig. 1, *E* and *F*). Although broad sites of H3K4me1 enrichment were present across the entire *Cyp27b1* locus and at the *Cyp27b1* promoter region in the absence of added hormone, enrichment sites unique to the introns of *Mettl1* and *Mettl21b* were also apparent (Fig. 1*E*). These potential enhancer regions in the kidney aligned precisely with the more punctate pCREB and VDR sites of occupancy, yet were completely absent in similar analyses of MSCs. Results obtained through ChIP-seq analysis of the histone activity mark H3K9ac revealed similar profiles with the exception that PTH up-regulated while FGF23 strongly suppressed H3K9ac enrichment; 1,25(OH)$_2$D$_3$ was without effect (Fig. 1*F*). These results suggest that both pCREB and VDR localize to unique and potentially active enhancers within specific introns of *Mettl1* and *Mettl21b* and that the H3K9ac mark appears to be directionally regulated by PTH and FGF23 as might be expected, revealing significant activity for both of these hormones. Notably, ChIP-seq analysis of H3K9ac enrichment in kidney extracts from two mouse models of secondary hyperparathyroidism confirmed the profound effect of sustained high PTH at both the putative enhancers and at *Cyp27b1* itself (Fig. 1*G*) (25, 26). These results support the novel finding that the regulatory regions that mediate PTH, 1,25(OH)$_2$D$_3$, and perhaps FGF23 action are located in selected introns of the *Mettl1* and *Mettl21b* genes.

DNase I hypersensitivity sequencing (DHS) analysis of kidneys from untreated WT mice performed by the ENCODE Consortium revealed the presence of distinct chromatin-occupied sites across a broad region containing the *Cyp27b1* locus from *Tsfm* to *Tspan31* (Fig. 2*C*) (27). Although common DHS sites are seen in kidney and in many other tissues, only the kidney contained a unique DHS site within the *Mettl1* intron and three unique sites in the *Mettl21b* intron that aligned not only with exclusive kidney enhancer marks but also with specific sites of pCREB and VDR occupancy. A similar profile of RNA pol II occupancy was also apparent consistent with an additional typical feature of enhancers (Fig. 2*D*) (28). These findings support the hypothesis that the regions within the *Mettl1* and *Mettl21b* introns likely represent a tissue-specific regulatory module that mediates transcriptional control of *Cyp27b1* in the kidney by the three primary mineral-regulating endocrine hormones. Interestingly, this gene-dense region in which *Cyp27b1* resides is defined by two major CCCTC-binding factor (CTCF)-occupied sites (Fig. 2*B*) (29, 30), prompting an examination of each gene between these sites. Both *Cyp27b1* and *Mettl21b* but not *Mettl1* or any additional genes in the region were similarly regulated by PTH, FGF23, and 1,25(OH)$_2$D$_3$ (Fig. 3, *A* and *B*). Although mechanistically unproven, the presence of the two CTCF sites together with similarities in the regulation of both *Mettl21b* and *Cyp27b1* advance speculation that this region may represent or reside in a small topologically associated domain (31).

Deletion of the pCREB/VDR enhancers results in phenotypically unique strains of mice

To explore the functional capabilities of the putative regulatory regions, we utilized a CRISPR/Cas9 approach (32) to create mouse strains with a deletion in the single putative enhancer located in *Mettl1* (324 bp) (termed Mettl1-IKO or M1-IKO) and a more complex deletion that removed the three putative enhancers located in *Mettl21b* (5.5 kb) (termed Mettl21b-IKO or M21-IKO) (Fig. 4*A*). We also generated a floxed *Cyp27b1* mouse through traditional homologous recombination methods and created a global *Cyp27b1*-deficient mouse (C27KO)

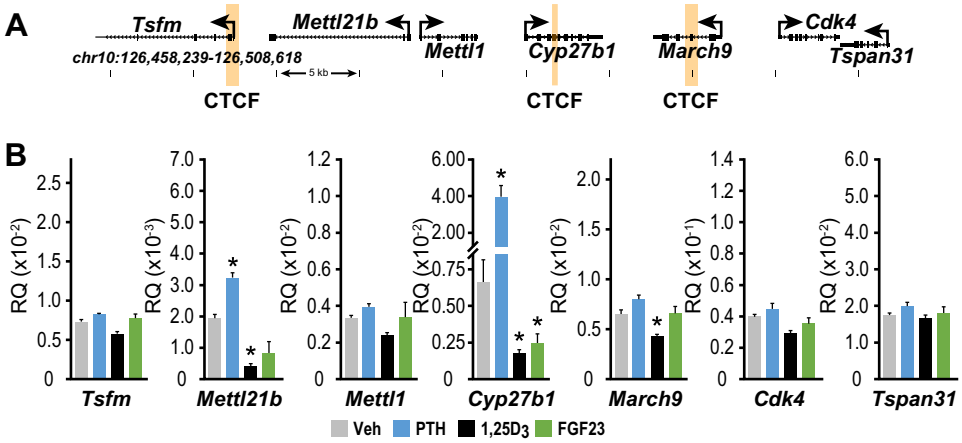

Figure 3. Co-regulation of neighboring genes within the CTCF boundaries. *A,* schematic of CTCF-binding locations (*yellow boxes*) in the *Cyp27b1* locus. *B,* gene expression in 8–9-week-old C57BL/6 wild-type mice of *Tsfm*, *Mettl21b*, *Mettl1*, *Cyp27b1*, *March9*, *Cdk4*, and *Tspan31* after treatment with ethanol/PBS vehicle (*Veh*, *gray*, $n = 6$), 230 ng/g bw PTH for 1 h (*PTH*, *blue*, $n = 6$), 10 ng/g bw $1,25(OH)_2D_3$ (*1,25D3*, *black*, $n = 6$) for 6 h, or 50 ng/g bw FGF23 for 3 h (*FGF23*, *green*, $n = 6$). Data displayed as relative quantitation (*RQ*, mean ± S.E.) compared with *Gapdh*. *, $p < 0.05$ paired *t* test, treatment *versus* vehicle.

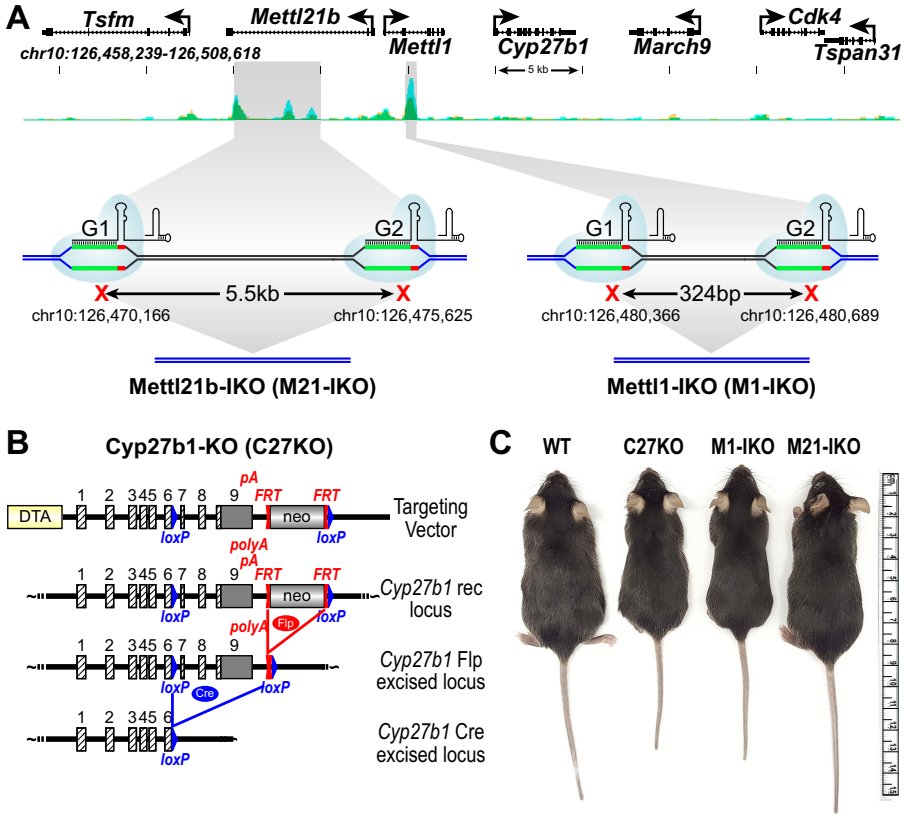

D

	Calcium (mg/dL)	Phosphate (mM)	PTH (pg/mL)	FGF23 (pg/mL)
WT	10.8 ± 0.1 (11)	2.4 ± 0.1 (11)	34.2 ± 4.9 (5)	194.2 ± 7.2 (5)
C27KO	7.7 ± 0.1* (8)	2.0 ± 0.1* (8)	3400.0 ± 495.4* (10)	6.2 ± 1.2* (9)
M1-IKO	8.6 ± 0.2* (12)	1.8 ± 0.1* (12)	2633.4 ± 366.2* (8)	6.7 ± 2.6* (7)
M21-IKO	11.5 ± 0.1* (8)	2.2 ± 0.1 (8)	56.4 ± 3.4* (10)	87.3 ± 6.0* (9)

Figure 4. Genomic knock-out of unique enhancers. *A,* schematic of CRISPR targeting in the *Cyp27b1* locus. VDR ChIP-seq data are shown as a reference. *Highlighted regions* were excised using two CRISPR-guide RNAs located at the indicated chromosome position. *B,* schematic of the Cyp27b1KO (*C27KO*) mouse targeting strategy. *C,* photograph of gross mouse size and length. *D,* table of serum calcium (mg/dl), phosphate (mM), PTH (pg/ml), and FGF23 (pg/ml) with *n* values indicated in *parentheses*. One-way ANOVA with multiple comparison Tukey post test: *, $p < 0.05$ KO *versus* WT.

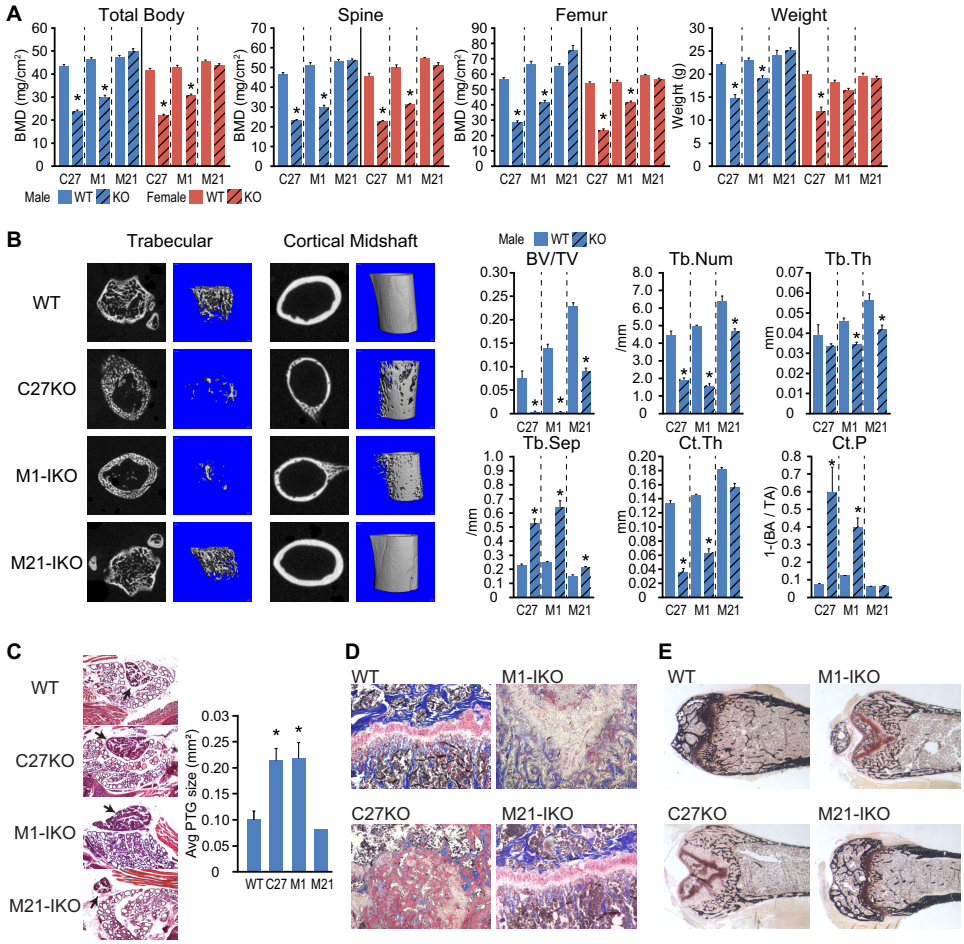

Figure 5. Skeletal phenotyping of the M1-IKO and M21-IKO mice. *A,* BMD measurements in total body, spine, and femur as well as weight measurements for male (*blue*) and female (*red*) in wild-type (*WT, solid bars, n* = 12) and C27KO (*n* = 6), M1-IKO (*n* = 14), and M21-IKO (KO, *striped, n* = 11) mice. *, $p < 0.05$ paired *t* test, KO *versus* WT. *B*, μCT images (*left*) and quantification (*right*) for bone volume/trabecular volume (*BV/TV*), trabecular number (*Tb.Num*), trabecular thickness (*Tb.Th*), trabecular separation (*Tb.Sep*), cortical thickness (*Ct.Th*), and cortical porosity (*Ct.P*). All mice were male (*blue*) in wild-type (*WT, solid bars*) and C27KO, M1-IKO, and M21-IKO (KO, *striped*) mice. *n* = 6 for all genotypes. *, $p < 0.05$ paired *t* test, KO *versus* WT. *C,* parathyroid gland hypertrophy is shown in thyroid sections. Parathyroid stains are *dark red*, location denoted by *black arrows*. Quantification by ImageJ software for each image (*n* = 3, M21 *n* = 1). *D,* trichrome staining of the femoral head and growth plate from WT, C27KO, M1-IKO, and M21-IKO mice (×4 magnification). Growth plate (*red*) and collagen (*blue*) is present and normal in WT and M21-IKO and is absent in C27KO and M1-IKO. *E,* von Kossa staining of the femoral head and growth plate (×2 magnification). Calcium (*black*) staining is present and normal in WT and M21-IKO and is decreased in C27KO and M1-IKO.

analogous to that reported by St-Arnaud and co-workers (26) (Fig. 4*B*). Visual inspection of each strain revealed that M21-IKO mice were similar to their WT counterparts, whereas M1-IKO mice were smaller and phenotypically similar to C27KO mice (Fig. 4*C*). Both of the latter two strains were extremely frail with mortality rates considerably higher than WT mice. Blood calcium and phosphate levels were similar in both M21-IKO and WT mice, whereas PTH levels were slightly elevated, and FGF23 levels were approximately half (Fig. 4*D*). In contrast, M1-IKO and C27KO mice displayed debilitating hypocalcemia and hypophosphatemia, highly elevated PTH levels, and a near absence of FGF23. Systemic parameters in the three mouse strains correlated directly with BMD measurements (Fig. 5*A*). μCT analysis, parathyroid gland hypertrophy, growth plate abnormalities, and mineralization (Fig. 5, *B–E*) indicated that M1-IKO and C27KO mice were similar, although the profile seen in the C27KO mouse was more extreme. Interestingly, differences in the skeletal phenotype of the M21-IKO mice from WT mice were limited to the trabecular compartment (Fig. 5*B*), potentially due to a bone remodeling issue as mineralization appeared intact (Fig. 5*E*).

Endocrine control of Cyp27b1 expression is altered in M1-IKO and M21-IKO kidneys

The different phenotypes of the M1-IKO and M21-IKO mice suggested that the regions in *Mettl1* and *Mettl21b* genes were responsible for distinct regulatory functions at the *Cyp27b1* gene. To examine this hypothesis, we assessed the steady-state expression of *Cyp27b1* and also the ability of each of the three hormones to regulate *Cyp27b1* expression in C27KO, M1-IKO, and M21-IKO mice (Fig. 1*A*). This latter test was executed to determine whether the gene remained sensitive to each individual hormone (Fig. 1*A*) but not to assess any potential physiological impact. Basal levels of *Cyp27b1* were strikingly elevated in C27KO mice compared with controls (Fig. 6, *A* and *B*) because, although the gene transcribes a mutant, truncated *Cyp27b1* RNA and non-functional enzyme (26), RNA production, and regulation remained fully intact. Interestingly, although high

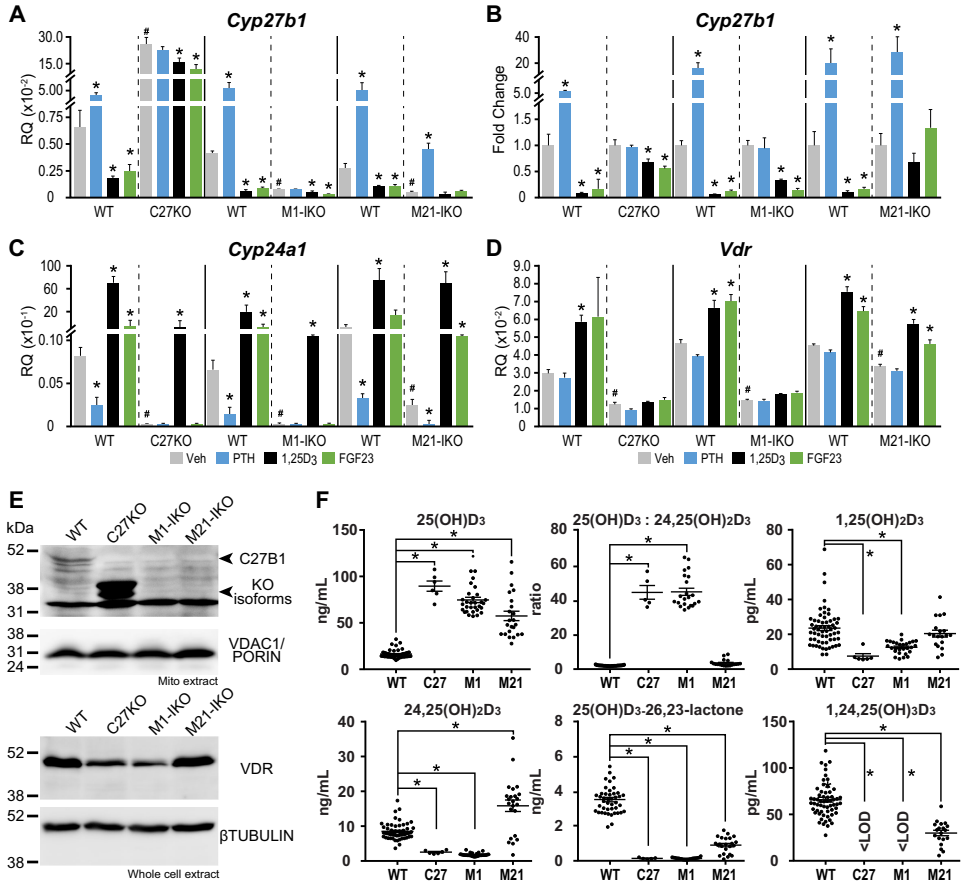

Figure 6. Gene expression and vitamin D metabolite levels. Gene expression of *Cyp27b1* (*A*), (*B, Cyp27b1* treatment fold change compared with vehicle), *Cyp24a1* (*C*), *Vdr* (*D*) after treatment in 8–9-week-old C27KO, M1-IKO, and M21-IKO mice compared with WT littermates with ethanol/PBS vehicle (*Veh, gray, n* = 6), 230 ng/g bw PTH for 1 h (*PTH, blue, n* = 6), 10 ng/g bw 1,25(OH)$_2$D$_3$ (*1,25D$_3$, black, n* = 6) for 6 h, or 50 ng/g bw FGF23 for 3 h (*FGF23, green, n* = 6). Data displayed as relative quantitation (*RQ*, mean ± S.E.) compared with *Gapdh*. *, $p < 0.05$ paired *t* test, treatment *versus* vehicle. #, $p < 0.05$ paired *t* test, KO Veh *versus* WT Veh. *E,* Western blot analysis of CYP27B1 protein expression from mitochondrial extracts compared with loading control VDAC1/PORIN protein expression (*top*). VDR protein expression compared with β-TUBULIN protein from whole-cell extract (*bottom*). *F,* vitamin D serum metabolite concentrations for WT (*n* = 60), C27KO (C27, *n* = 6), M1-IKO (M1, *n* = 28), M21-IKO (M21, *n* = 19) for 25(OH)D$_3$ in individual animals (ng/ml), 1,25(OH)$_2$D$_3$ (pg/ml), 24,25(OH)$_2$D$_3$ (ng/ml), ratio of 25(OH)D$_3$/24,25(OH)$_2$D$_3$; 25(OH)D$_3$-26,23-Lactone (ng/ml) and 1,24,25(OH)$_3$D$_3$ (pg/ml) displayed as scatter plots (mean ± S.E.). One-way ANOVA with multiple comparison Tukey post test: *, $p < 0.05$ KO *versus* WT. 1,24,25(OH)$_3$D$_3$ was below the limit of detection (<LOD) for C27KO and M1-IKO.

residual levels of PTH in C27KO mice limited response of *Cyp27b1* to exogenous PTH administration, these high levels were unable to prevent FGF23 or 1,25(OH)$_2$D$_3$ from modestly suppressing *Cyp27b1* (Fig. 6, *A* and *B*). In contrast, although WT mice retained normal sensitivity to each of the three hormones, basal *Cyp27b1* expression in M1-IKO mice was strikingly reduced (95%) (Fig. 6*A*). Because both C27KO and M1-IKO mouse strains exhibit high PTH levels, the only explanation for the dramatic up-regulation of *Cyp27b1* expression in C27KO mice coincident with the dramatic down-regulation of the gene in M1-IKO mice is that in the latter strain sensitivity to PTH has been lost. Loss of circulating PTH via thyroparathyroidectomy reduces basal production of 1,25(OH)$_2$D$_3$, an effect that has been previously documented (7). *Cyp27b1* expression in both C27KO and M1-IKO mice exhibits a similar pattern of sensitivity to FGF23 and 1,25(OH)$_2$D$_3$ suppression and loss of sensitivity to PTH induction. Therefore, it is clear that the loss of PTH sensitivity in the M1-IKO mouse is due to deletion of the *Mettl1* intronic region. M21-IKO mice exhibit a similar but more limited decrease in basal *Cyp27b1* expression (75%), retain complete sensitivity to PTH, yet are insensitive to both FGF23 and 1,25(OH)$_2$D$_3$ treatment (Fig. 6, *A* and *B*). Thus, the region that is deleted in the M21-IKO mice appears to contain an independent regulatory feature that influences basal *Cyp27b1* expression, perhaps due to the actions of an additional unknown positive factor analogous to that of PTH, as well as regions that mediate suppression by FGF23 and 1,25(OH)$_2$D$_3$. The co-regulation of *Mettl21b* (Fig. 3) is also lost as a result of these individual deletions, demonstrating that the activities of these enhancers are potentially shared (data not shown). Importantly, CYP27B1 protein levels in M1-IKO and M21-IKO kidneys were also strongly suppressed (Fig. 6*E*). As expected, high levels of non-functional, mutated CYP27B1 protein were seen in C27KO kidneys, migrating more rapidly than the WT protein due to loss of exons 7–9 (Fig. 6*E*).

Basal suppression of kidney Cyp27b1 causes secondary suppression of Cyp24a1 and Vdr

Loss of circulating 1,25(OH)$_2$D$_3$ and up-regulation of PTH in C27KO mice results in suppression of *Cyp24a1* and *Vdr* expression (33). *Cyp24a1* expression was dramatically down-regulated in both C27KO and M1-IKO mice (Fig. 6*C*), likely due to

the high levels of PTH and low levels of FGF23 (Fig. 4*D*). Although *Cyp24a1* remained sensitive to up-regulation by $1,25(OH)_2D_3$ in the kidneys of each strain, both FGF23 induction and PTH suppression appeared to be fully quenched. Surprisingly, M21-IKO mice also exhibit *Cyp24a1* suppression, although this level was less dramatic. Nevertheless, *Cyp24a1* retained sensitivity to PTH down-regulation and FGF23 and $1,25(OH)_2D_3$ up-regulation. As basal CYP24A1 protein levels were undetectable in WT, C27KO, M1-IKO, and M21-IKO mice, direct assessment of protein down-regulation was not possible (data not shown). The more modest secondary reduction in *Cyp24a1* expression in M21-IKO mice is likely due to the limited increase in PTH but also to a reduction in FGF23, which would limit *Cyp24a1* expression (considered below) (10). *Vdr* was also suppressed in C27KO and M1-IKO kidneys (Fig. 6*D*), a reduction that was confirmed directly at the protein level (Fig. 6*E*). The modest up-regulation of *Vdr* by $1,25(OH)_2D_3$ and FGF23 seen in WT mice appears to be lost in C27KO and M1-IKO mice (Fig. 6*D*), perhaps due to the low calcemic state of both mouse strains (34). Collectively, these studies of *Cyp27b1*, *Cyp24a1*, and *Vdr* expression in C27KO, M1-IKO, and M21-IKO mice suggest that their phenotypes are due to aberrant basal *Cyp27b1* expression, selective loss of hormonal regulation in the kidney, and complex reciprocal homeostatic regulation of *Cyp24a1*. These activities appear to be intrinsic to the regulatory regions themselves, as ChIP-seq analysis of the *Cyp27b1* locus in both M1-IKO and M21-IKO mice revealed that the deletion of either the *Mettl1* or the *Mettl21b* intronic enhancer (*underlined in red* in Fig. 7, *A* and *B*) had no effect on either VDR or pCREB binding in the opposite regulatory region. In this analysis, VDR binding in the C27KO mouse was used as a control, as VDR levels in the kidneys of both C27KO and M1-IKO mice show similar down-regulation and thus impact the level of genomic VDR binding in ChIP-seq analyses comparably. A similar analysis of epigenetic signature marks in these mice also revealed a lack of cross-structural alteration (data not shown). Importantly, as highlighted in Fig. 6, *A* and *B*, *Cyp27b1* expression in M1-IKO mice is insensitive to the high circulating levels of PTH, and this is demonstrated amply through the lack of H3K9ac enrichment that is seen in both C27KO and VDRKO mice (Fig. 7*C*).

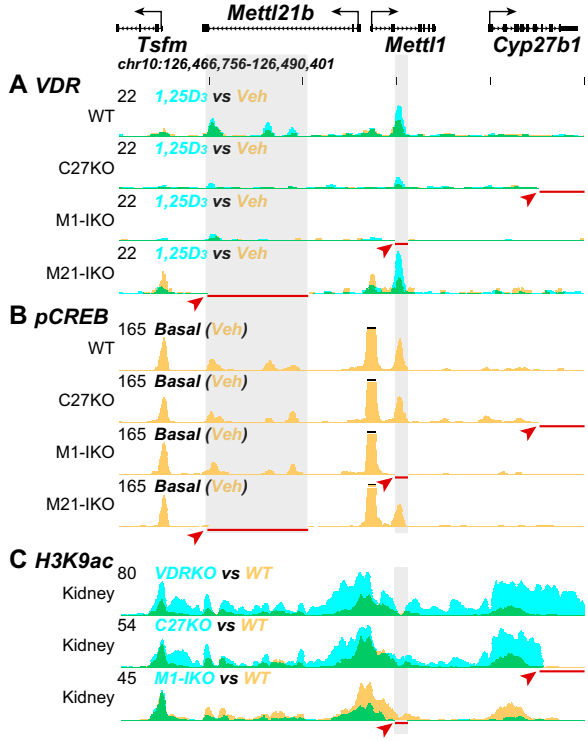

Figure 7. M1-IKO and M21-IKO enhancer genomic occupancy. Overlaid ChIP-seq data tracks for VDR (*A*) and pCREB (*B*) from mouse kidney in wild-type (*WT*), C27KO, M1-IKO, or M21-IKO mice displayed as either basal or vehicle (*Veh*) (*yellow*, $n = 3$) or treated (*blue*, $n = 3$) with 10 ng/g bw $1,25(OH)_2D_3$, for 1 h. *C*, H3K9ac data in VDRKO (*blue*), Cyp27b1KO mice (C27KO, *blue*), or M1-IKO mice (M1-IKO, *blue*) *versus* wild-type (*WT, yellow*). Overlapping track data appear as *green*. Overlapping track data appear as *green*. Regions of interest are highlighted in *light gray boxes*. Deleted genomic regions denoted by *red line* and *red arrowhead*. Genomic location and scale are indicated (*top*) and maximum height of tag sequence density for each data track is indicated on the *y* axis (*top left each track*, normalized to input and 10^7 tags). Gene transcriptional direction is indicated by an *arrow* and exons by *boxes*.

Basal suppression of Cyp27b1 expression in M1-IKO but not M21-IKO kidneys results in altered vitamin D metabolite levels

We utilized LC-MS/MS techniques to determine $25(OH)D_3$, $24,25(OH)_2D_3$, and $25(OH)D_3$-26,23-lactone levels, as well as a novel antibody-based LC-MS/MS method to measure $1,25(OH)_2D_3$ and $1,24,25(OH)_3D_3$ levels in the blood of WT, C27KO, M1-IKO, and M21-IKO mice (Fig. 6*F*). $25(OH)D_3$ levels in C27KO, M1-IKO mice were well above those of WT littermate controls with the highest levels observed in the C27KO mice. $24,25(OH)_2D_3$ and $25(OH)D_3$-26,23-lactone levels, however, were extremely low in the C27KO and M1-IKO mice giving rise to elevated $25(OH)D_3/24,25(OH)_2D_3$ ratios consistent with reduced *Cyp24a1* expression and *in vivo* enzyme function. Low circulating levels of $1,25(OH)_2D_3$ and $1,24,25(OH)_3D_3$ (<LOD) in these animals suggest that reduced *Cyp24a1* expression arises from either a lack of CYP27B1 itself (C27KO) or its PTH-responsive enhancer (M1-IKO). Although M21-IKO mice exhibited higher levels of expression of *Cyp24a1* relative to C27KO and M1-IKO mice, expression levels remained lower than WT (Fig. 6*C*). While $25(OH)D_3$ was also elevated in M21-IKO animals, $24,25(OH)_2D_3$ was 2-fold greater than in its WT counterparts. The $25(OH)D_3/24,25(OH)_2D_3$ ratio suggests that the rise in $24,25(OH)_2D_3$ results from elevated $25(OH)D_3$ substrate, but we note that the mean ratio is slightly elevated indicating a somewhat blunted CYP24A1 function. Further analysis of downstream $25(OH)D_3$-26,23-lactone levels revealed a 4-fold lower concentration than WT and a 20-fold increase in the $25(OH)D_3/25(OH)D_3$-26,23-lactone ratio (data not shown). $1,24,25(OH)_3D_3$ levels were also 3-fold lower in the M21-IKO animals, despite near-normal $1,25(OH)_2D_3$. Taken together, the intermediate level of *Cyp24a1* expression observed in M21-IKO animals appears to manifest as altered progression of metabolism through to downstream catabolites, rather than the extreme reduction in serum $24,25(OH)_2D_3$, $25(OH)D_3$-26,23-lactone, and $1,24,25$-$(OH)_3D_3$ levels observed in C27KO and M1-IKO mice. $1,25(OH)_2D_3$ concentrations are consistent with the overall systemic and skeletal phenotypes of each of the mouse strains. These results suggest that whereas the general phenotype of M21-IKO mice appears normal, minor changes in the skeleton (Fig. 5) together with alterations

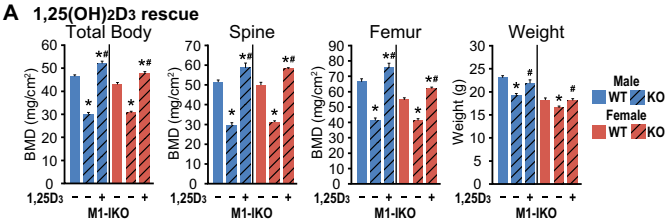

B Vitamin D_3 deficiency

D_3 in Diet		25-OH-D_3 (ng/mL)	24,25-$(OH)_2D_3$ (ng/mL)	Calcium (mg/dL)	Phosphate (mM)	PTH (pg/mL)	FGF23 (pg/mL)
+	WT	13.4 ± 1.9 (8)	7.5 ± 2.0 (8)	10.8 ± 0.3 (8)	2.4 ± 0.1 (8)	34 ± 4.9 (8)	194.2 ± 13.2 (8)
	M1-IKO	86.2 ± 12.0* (7)	1.49 ± 0.2* (7)	8.6 ± 0.3 (7)	1.8 ± 0.1* (7)	1560 ± 307.4* (7)	6.7 ± 1.8*(7)
	C27KO	78.5 ± 10.6* (5)	1.81 ± 0.4* (5)	7.7 ± 0.3 (5)	2.1 ± 0.1 (5)	3044.9 ± 779.2* (5)	6.2 ± 2.5* (5)
−	WT	3.12 ± 0.1 (12)	0.2 ± 0.1 (12)	10.8 ± 0.3 (12)	2.4 ± 0.1* (12)	29.0 ± 2.9 (12)	164.9 ± 13.9* (12)
	M1-IKO	7.04 ± 1.6* (8)	0.63 ± 0.3* (8)	7.1 ± 0.3 (8)	1.8 ± 0.1* (8)	3396.7 ± 287.5* (8)	6.8 ± 1.5* (8)
	C27KO	5.77 ± 0.6* (5)	0.84 ± 0.2* (5)	7.3 ± 0.4 (5)	1.6 ± 0.1* (5)	3030.6 ± 631.4* (5)	8.9 ± 3.6* (5)

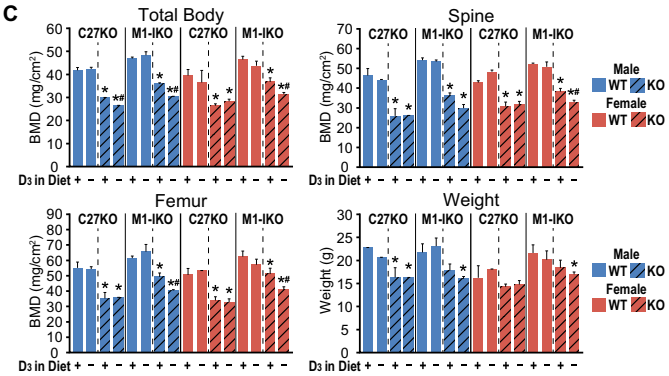

Figure 8. Dietary treatment for M1-IKO mice. *A,* bone mineral density (*BMD*) measurements in total body, spine, and femur as well as weight measurements for male (*blue*) and female (*red*) in wild-type (*WT, solid bars*) and C27KO or M1-IKO (*KO, striped*) mice fed chow diet (−) or chow supplemented with 1 ng/g 1,25$(OH)_2D_3$ (+). Two-way ANOVA with multiple comparison Tukey post-test is shown. $n = 4$ for both sex and treatment. *, $p < 0.05$ KO *versus* WT. #, $p < 0.05$ 1,25D_3 diet *versus* chow. *B, table* of serum 25$(OH)D_3$ (ng/ml), 24,25$(OH)_2D_3$ (ng/ml), calcium (mg/dl), phosphate (mM), PTH (pg/ml), and FGF23 (pg/ml) in mice fed a purified diet containing vitamin D_3 (+) *versus* purified diet without vitamin D_3 (−) with *n* values indicated in *parentheses.* One-way ANOVA with multiple comparison Tukey post test: *, $p < 0.05$ KO *versus* WT. *C,* BMD measurements in total body, spine, and femur as well as weight measurements for male (*blue*) and female (*red*) in wild-type (*WT, solid bars*) and C27KO or M1-IKO (*KO, striped*) mice fed a purified diet containing vitamin D_3 (+) *versus* purified diet without vitamin D_3 (−). $n = 4$ for both sex and treatment. Two-way ANOVA with multiple comparison Tukey post-test is shown. *, $p < 0.05$ KO *versus* WT. #, $p < 0.05$ diet *versus* diet without vitamin D_3.

in both systemic (Fig. 4*D*) and vitamin D metabolic (Fig. 6*F*) profiles appear instrumental in sustaining the near normal levels of 1,25$(OH)_2D_3$, thereby preserving mineral homeostasis in these particular mice. We emphasize that C27KO and M1-IKO mice were unable to produce 1,24,25$(OH)_3D_3$, a metabolite that is measured in the blood of WT mice and also appears to be produced at low but significant levels in M21-IKO mice. This represents the first robust measurement of a metabolite that, while comprising the first catabolic product of CYP24A1 action on 1,25$(OH)_2D_3$, is also the second most biologically active vitamin D metabolite known (35, 36). Finally, the central importance of low 1,25$(OH)_2D_3$ in the aberrant phenotype in the M1-IKO mouse was confirmed by the ability of a diet containing exogenously added 1,25$(OH)_2D_3$ to rescue the abnormal skeletal phenotype of the M1-IKO mouse (Fig. 8*A*). An additional experiment in which vitamin D was removed from the diet, thereby reducing circulating 25$(OH)D_3$ levels, revealed that although the phenotype of the C27KO mouse was unaffected by this treatment regimen, as expected of a mouse that cannot make 1,25$(OH)_2D_3$, the phenotype of the M1-IKO mouse worsened and after 5 weeks was similar to that of the C27KO mouse (Fig. 8, *B* and *C*).

Repressive abilities of the intronic Mettl21b enhancer

Similarities between the ability of 1,25$(OH)_2D_3$ and FGF23 to suppress *Cyp27b1* expression in the kidney and their union in the intron of *Mettl21b* prompted the idea that 1,25$(OH)_2D_3$ might suppress *Cyp27b1*, at least in part, through FGF23 by inducing transcription of the *Fgf23* gene and raising its blood levels, an established function of 1,25$(OH)_2D_3$ (37, 38). Additional evidence includes the following. 1) ChIP-seq studies across the *Cyp27b1* locus suggested that although both PTH induced and FGF23 suppressed H3K9ac enrichment within the intronic regions of *Mettl1* and *Mettl21b* and at the *Cyp27b1* promoter, 1,25$(OH)_2D_3$ was without effect at this time point (Fig. 1*F*). 2) a reduction of VDR binding within the *Mettl21b* intron in the M1-IKO mouse due to *Vdr* down-regulation did not appear to limit the ability of either 1,25$(OH)_2D_3$ or FGF23 to suppress *Cyp27b1* expression (Fig. 7). To test this hypothesis, we correlated the ability of 1,25$(OH)_2D_3$ to suppress *Cyp27b1* expression over time in WT kidneys with its ability to induce *Fgf23* in bone. The results revealed that following an acute but modest up-regulation of *Cyp27b1* expression, 1,25$(OH)_2D_3$ provoked a rapid suppression of *Cyp27b1* that reached near baseline within 4–6 h (Fig. 9*A*). This suppression was fully sustained for at least 24 h, an unusual feature of 1,25$(OH)_2D_3$ activity alone, and likely much longer given previous studies (39). Importantly, *Fgf23* transcripts were also induced by 1,25$(OH)_2D_3$ in the skeleton within this same time frame (Fig. 9*B*). Based upon this finding, we then correlated these temporal responses with serum levels of PTH and FGF23 as well as calcium and phosphate. Although PTH was mildly suppressed by 1,25$(OH)_2D_3$, FGF23 was increased from a residual baseline of 200 to ~1700 pg/ml at 12 h (Fig. 9*A*). Both calcium and phosphate were also induced by 1,25$(OH)_2D_3$ within this time period, an *in vivo* response to the hormone that has been well-established. These results support the idea that both 1,25$(OH)_2D_3$ and FGF23 may act either sequentially or together to suppress *Cyp27b1* expression through a sustained effect mediated by the up-regulation of FGF23. It is worth noting that the mobilization of phosphate may also play an important role because both 1,25$(OH)_2D_3$ and phosphate are the most striking regulators of FGF23 that are currently known (40). A similar time course of *Cyp27b1* response to 1,25$(OH)_2D_3$ was also seen in M1-IKO kidneys (Fig. 9*E*), although this response was less robust because the basal expression of *Cyp27b1* and serum levels of FGF23 are already highly suppressed (Figs. 4*D* and 6*A*). In WT mice, the temporary reduction of FGF23 and elevation in PTH allows PTH to transiently increase *Cyp27b1* expression. However, *Cyp27b1* expression is not acutely increased in the M1-IKO mice due to its insensitivity to PTH. Importantly, although this study suggests that the suppression of *Cyp27b1* by 1,25$(OH)_2D_3$ may involve the induction of FGF23 either directly by the hormone or via its mobilization of phosphate, proof of this hypothesis

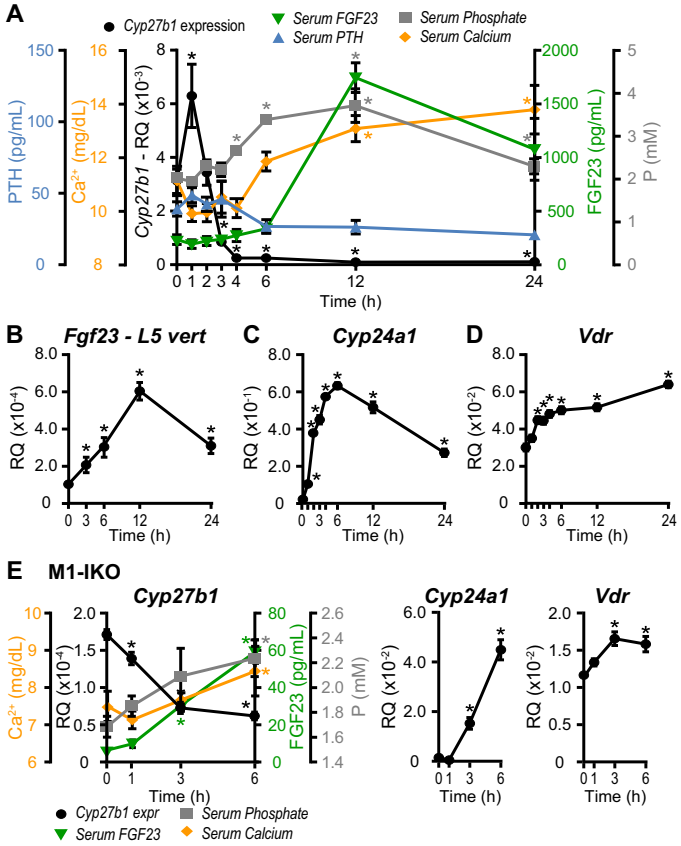

Figure 9. Time course of $1,25(OH)_2D_3$ repression of *Cyp27b1*. *A*, overlaid data for *Cyp27b1* gene expression in the kidney (*black*), serum FGF23 (*green*), serum PTH (*blue*), serum phosphate (*gray*), and serum calcium (*orange*) in 8–9-week-old wild-type C57BL/6 mice after 10 ng/g dose of $1,25(OH)_2D_3$ for 0, 1–4, 6, 12, and 24 h. *Fgf23* (*B*) expression from the L5 vertebrae and *Cyp24a1* (*C*) and *Vdr* (*D*) gene expression from the kidney using same time points. Gene expression data displayed as relative quantitation (*RQ*, mean ± S.E.) compared with *Gapdh*. $n = 6$ for all time points. One-way ANOVA with multiple comparison Tukey post-test: *, $p < 0.05$ time point *versus* 0 h. *E*, overlaid data for *Cyp27b1* gene expression as in *A* for the M1-IKO mice, as well as *Cyp24a1* and *Vdr* gene expression. PTH was excluded due to extremely high and unchanged serum levels.

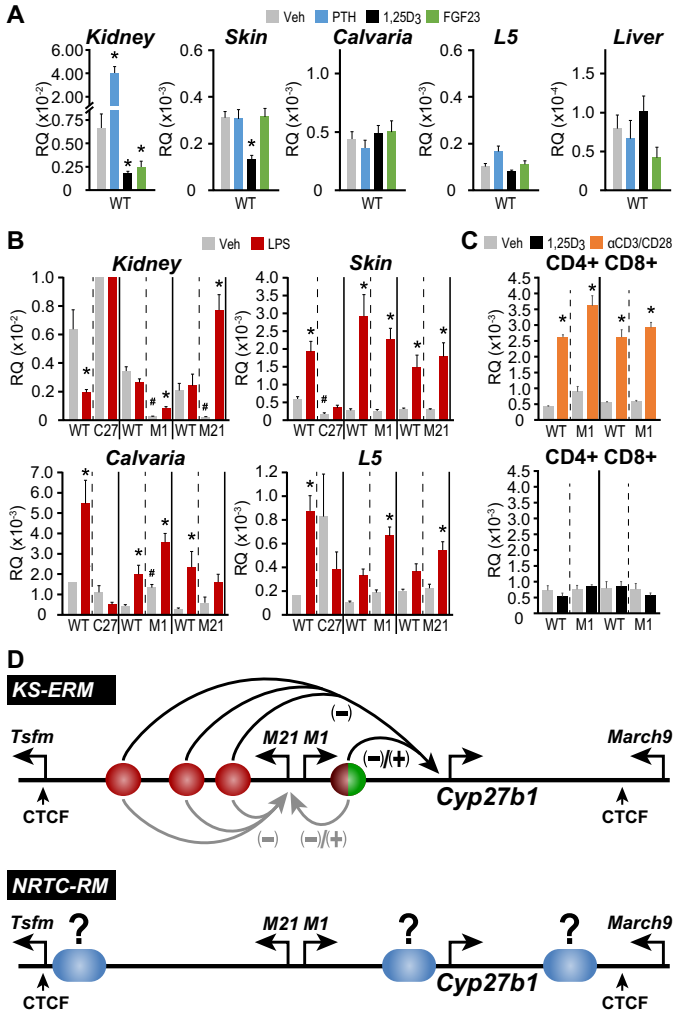

Figure 10. Non-renal target cell expression of *Cyp27b1*. *A*, gene expression of *Cyp27b1* after treatment in 8–9-week-old C57BL/6 wild-type mice with ethanol/PBS vehicle (*Veh, gray*, $n = 6$), 230 ng/g bw PTH for 1 h (*PTH, blue*, $n = 6$), 10 ng/g bw $1,25(OH)_2D_3$ (*1,25D3, black*, $n = 6$) for 6 h, or 50 ng/g bw FGF23 for 3 h (*FGF23, green*, $n = 6$) examined in kidney, skin, calvaria, L5 vertebrae, and liver. *B*, *Cyp27b1* gene expression in kidney, skin, calvaria, and L5 vertebrae after treatment with 10 mg/kg lipopolysaccharides (*LPS, red*, $n = 6$) for 6 h *versus* vehicle (*Veh, gray*, $n = 6$). *C*, *Cyp27b1* gene expression in $CD4^+$ and $CD8^+$ T cells in M1-IKO or WT littermate mice activated with α-CD3/CD28 antibody for 3 h (*left, orange*, $n = 6$) or 100 nM $1,25(OH)_2D_3$ for 3 h (*right, black*, $n = 6$) *versus* vehicle (*Veh, gray*, $n = 6$). Data displayed as relative quantitation (*RQ*, mean ± S.E.) compared with *Gapdh*. *, $p < 0.05$ paired *t* test, treatment *versus* vehicle. *D*, schematic diagram of the KS-ERM) incorporating the M1 and M21 enhancer control regions compared with the NRTC-RM. Repressive elements are shown in *red*; activating elements are shown in *green*, and unknown elements are shown in *blue*.

will require delineation of the exact sites of FGF23 action in the *Mettl21b* intron following identification of the transcription factor(s) involved and/or elimination of the ability of $1,25(OH)_2D_3$ to up-regulate *Fgf23* expression.

Regulation of Cyp27b1 expression in NRTCs is functionally unique from the kidney

Previous studies have suggested that *Cyp27b1* is expressed in a number of NRTCs and may be responsible for local conversion of $25(OH)D_3$ to $1,25(OH)_2D_3$ (4). However, its expression does not appear to be regulated by either PTH or FGF23 and perhaps only modestly by $1,25(OH)_2D_3$. *Cyp27b1* expression is extremely low in NRTCs, and these hormones do not regulate *Cyp27b1* in skin, bone, liver, and other specific cell types, although $1,25(OH)_2D_3$ modestly suppressed *Cyp27b1* in the skin and in thyroparathyroid gland tissue (TPTG) (Fig. 10*A* and 11*A*). Based upon ChIP-seq analysis of MSCs (Figs. 1 and 2), we reasoned that the absence of *Cyp27b1* regulation by PTH and FGF23 and, in specific NRTC cases, by $1,25(OH)_2D_3$ could be explained by the absence of the endocrine enhancers. To test this idea, we compared the basal expression levels of *Cyp27b1* in several NRTCs from C27KO, M1-IKO, and M21-IKO mice with those of individual littermate controls. Basal levels of *Cyp27b1* expression in skin, calvaria, and L5 vertebrae were unaffected by either of the two genomic deletions (Fig. 10*B*). Interestingly, both basal and *ex vivo* T cell receptor-inducible levels of *Cyp27b1* expression in T cells isolated from either WT or M1-IKO spleens were also unaffected (Fig. 10*C*) (41). These general findings provide key support for the idea that the regulatory module that mediates the actions of PTH, FGF23, and $1,25(OH)_2D_3$ at *Cyp27b1* is absent in NRTCs and thus prevents similar regulation by the three endocrine hormones. Based upon tissue selectivity, we have termed this the kidney-specific

endocrine regulatory module (KS-ERM). Surprisingly, although the calcium and phosphate hormones are unable to control *Cyp27b1* expression in NRTCs, the ability of the inflammatory modulator LPS to induce *Cyp27b1* was fully apparent (Fig. 10*B*). LPS induction of *Cyp27b1* expression has been previously described, particularly in immune cells such as macrophages, where it is suggested to be involved in the ability of vitamin D to modulate both innate and acquired immunity (42). Importantly, the ability of LPS to induce the *Cyp27b1* gene in these cell types was unaffected by the enhancer deletions introduced into the M1-IKO and M21-IKO mice, although LPS activity appeared to be potentially unmasked in the kidneys of these mutant mice as a consequence of the reduced basal *Cyp27b1* expression in both strains (Fig. 10*C*). We conclude that LPS and T cell receptor activation of *Cyp27b1* in distinct NRTCs is mediated by a regulatory region(s) we have termed the NRTC-regulatory module (NRTC-RM) whose location lies outside that defined by the two separate components of the KS-ERM (Fig. 10*D*).

Cyp27b1 locus in TPTG tissue contains signatures of both NRTCs and renal cells

Cyp27b1 is expressed at reduced levels in isolated cells of the parathyroid gland (PTG) and in *ex vivo* cultures of both PTG cells and organs of several species (43, 44). However, the regulatory properties of the *Cyp27b1* gene itself have not been explored in this tissue *in vivo*. We therefore examined in a concluding set of studies the potential for *Cyp27b1* regulation in the parathyroid gland, based upon the strong linkage between the function of this organ and its central involvement in the regulation of both $1,25(OH)_2D_3$ metabolism and mineral homeostasis. This was enabled by excising total TPTG tissue after hormone injection into WT, C27KO, M1-IKO, or M21-IKO mice and conducting both RNA expression and ChIP-seq analysis in this set of glands. Although the tissue is more complex, this approach allowed us to avoid time-consuming isolation methods and *ex vivo* culturing and to assess analyses directly from the mice. Although much has been made of vitamin D action to suppress expression of the PTH gene, loss of the VDR by selective gene knock-out in the parathyroid glands of mice has revealed only a minor impact on PTH expression, suggesting that the primary actions of vitamin D in this tissue remain to be understood (45). Of the three hormones and LPS administered to WT mice, only $1,25(OH)_2D_3$ was statistically active and modestly suppressed *Cyp27b1* expression (Fig. 11*A*). Loss of the enhancer in the M1-IKO mouse resulted in a striking suppression of *Cyp27b1* much like that seen in the kidney; this suppression was not seen in the TPTG of M21-IKO mice (Fig. 11, *A* and *B*). We therefore treated WT mice with a single dose of $1,25(OH)_2D_3$ and examined the *Cyp27b1* locus using ChIP-seq for the presence of the VDR at sites observed in the kidney (Fig. 1*D*). Despite the presence of the VDR at accepted target genes for $1,25(OH)_2D_3$ in the TPTG, including *Cyp24a1*, VDR occupancy was not detected anywhere within the *Cyp27b1* locus (data not shown). To explore further, we examined the epigenetic landscape surrounding the *Cyp27b1* gene in the TPTG, and we assessed the basal levels of the enhancer signature marks H3K4me1 and H3K9ac and compared them with those in the kidney and in MSCs. Although several minor similarities were apparent, neither of these epigenetic marks displayed a pattern consistent with that seen in the kidney (Fig. 11*C*). Similar to the kidney, H3K4me1 shows a minor enrichment in the M21-IKO region (*furthest left highlighted region*, Fig. 11*C*) as well as the M1-IKO region; however, H3K9ac is more comparable to the MSC control and devoid of activity in both regions. We then examined basal epigenetic H3K4me1 and H3K9ac landscapes across the *Cyp27b1* gene in TPTG tissue derived from either C27KO or M1-IKO mice and compared them with those obtained from their WT littermates (Fig. 11*D*). Although modest H3K4me1 enrichment was seen in a single region in the *Mettl21b* intron and perhaps in the *Mettl1* intron in these contrasting ChIP-seq analyses, there was no evidence of residual enrichment of either the H3K4me1 or H3K9ac activity marks in either intron. These results suggest that despite minor functional similarities, the *Cyp27b1* gene locus in the TPTG reflects an enhancer landscape that is more similar to NRTCs than to the kidney. We conclude that the KS-ERM is a control module unique to the kidney, providing regulatory capabilities at the *Cyp27b1* gene that mediate unique sensitivity to PTH, FGF23, and $1,25(OH)_2D_3$.

Discussion

The phenotypes of the mice carrying KS-ERM deletions contrast with those of WT mice and suggest that reduced expression of *Cyp27b1* stimulates striking adaptive homeostatic responses that involve the differential production of PTH and FGF23 as well as $1,25(OH)_2D_3$. These responses impact not only *Cyp27b1* and *Cyp24a1* expression but vitamin D metabolism as well and highlight both the genomic as well as homeostatic circuits that are essential for the maintenance of normal mineral balance. A summary of the key players involved in this homeostatic response and our working hypothesis is illustrated in Fig. 12*A*, where the physiological actions of PTH, FGF23, and $1,25(OH)_2D_3$ are likewise shown reflecting the specific mouse models that have been used to describe the interrelationships. Sites of activity controlled by the enhancers deleted in the M1-IKO and M21-IKO strains are also depicted as well. As documented, most of these models are functionally linked to the aberrant regulation of *Cyp27b1* expression or activity in the kidney, which leads to abnormal $1,25(OH)_2D_3$ production. Decreased circulating levels of $1,25(OH)_2D_3$ result in hypocalcemia and hypophosphatemia, prompting a rise in PTH and a suppression of FGF23. In the case of normal mice, homeostatic changes in PTH and FGF23 correct the underexpression of *Cyp27b1* and suppress *Cyp24a1* expression, raising blood $1,25(OH)_2D_3$ levels that together with PTH and FGF23 normalize extracellular calcium and phosphate metabolism.

In M1-IKO mice, however, and prompted by the down-regulation of *Cyp27b1*, the gene's up-regulation is disrupted due to the lack of *Cyp27b1* sensitivity to PTH. Thus, calcium and phosphate lowering persists, causing a sustained rise in PTH and a further decrease in FGF23. These two hormonal changes also suppress *Cyp24a1* expression that both decreases $1,25(OH)_2D_3$ turnover and compromises $24,25(OH)_2D_3$ and $1,24,25(OH)_3D_3$ production, thereby eliciting an elevation in $25(OH)D_3$ substrate levels. This rise may contribute to a

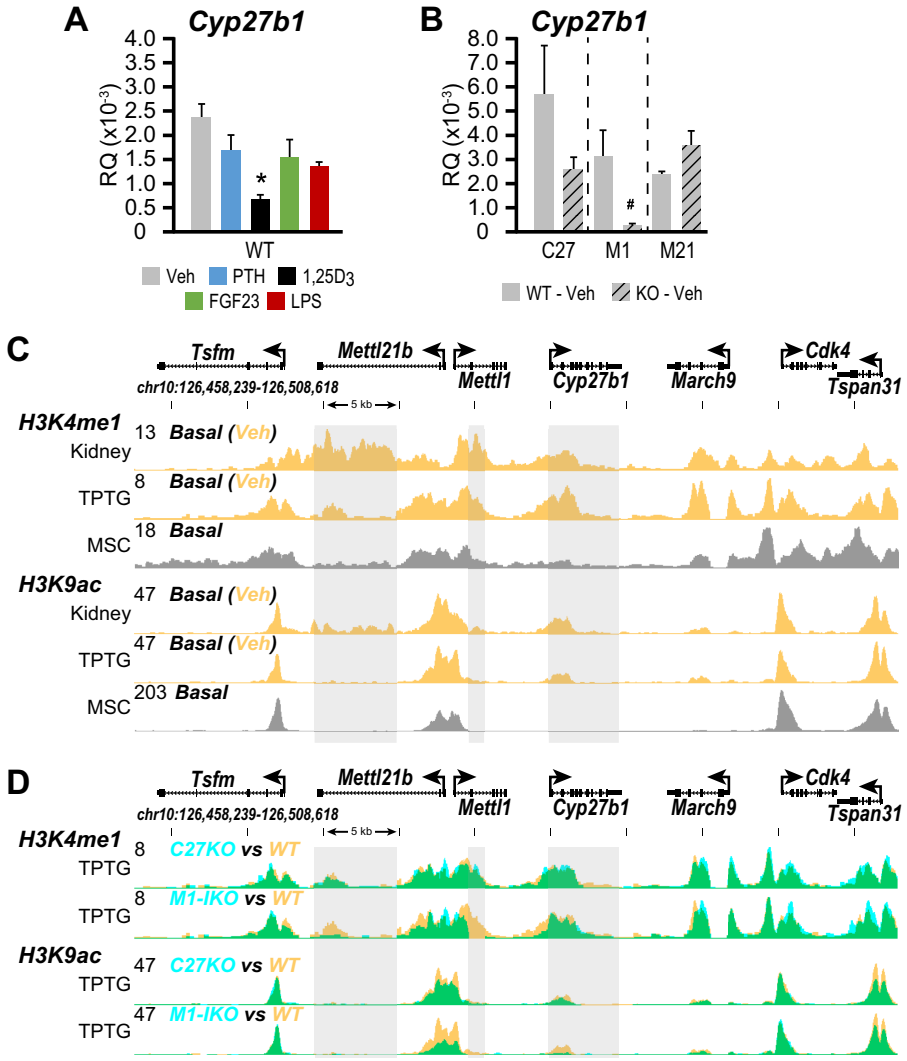

Figure 11. Parathyroid gland expression and genomic occupancy of *Cyp27b1*. *A*, gene expression of *Cyp27b1* after treatment in 8–9-week- old C57BL/6 wild-type mice with ethanol/PBS vehicle (*Veh, gray, n* = 6), 230 ng/g bw PTH for 1 h (*PTH, blue, n* = 6), 10 ng/g bw 1,25(OH)$_2$D$_3$ (*1,25D$_3$, black, n* = 6) for 6 h, 50 ng/g bw FGF23 for 3 h (*FGF23, green, n* = 6), or 10 mg/kg lipopolysaccharides (*LPS, red, n* = 6) examined in the TPTG. *, $p < 0.05$ paired *t* test, treatment *versus* vehicle. *B*, gene expression of *Cyp27b1* in C27KO, M1-IKO, and M21-IKO mice (*KO, striped, n* = 6) basally (vehicle) compared with wild-type (*WT, solid, n* = 6) littermates in the TPTG. *, $p < 0.05$ paired *t* test, KO *versus* WT. Data displayed as relative quantitation (*RQ*, mean ± S.E.) compared with *Gapdh*. Overlaid data tracks for genomic occupancy by ChIP-seq of H3K4me1 and H3K9ac basally (*yellow*) in kidney, TPTG, and MSC (*C*) or C27KO and M1-IKO (*blue*) *versus* WT (*yellow*) (*D*). Overlapping track data appear as *green*. Regions of interest are highlighted in *light gray boxes*. Genomic location and scale are indicated (*top*), and maximum height of tag sequence density for each data track is indicated on the *y* axis (*top left each track*, normalized to input and 10^7 tags). Gene transcriptional direction is indicated by an *arrow* and exons by *boxes*.

homeostatic effort to raise circulating blood levels of 1,25(OH)$_2$D$_3$, which is largely futile in the case of the M1-IKO mice. In contrast, the reduced expression of *Cyp27b1* in M21-IKO mice with retained gene sensitivity to PTH is sufficient to mediate appropriate up-regulation of 1,25(OH)$_2$D$_3$ to maintain a normal calcium and phosphate balance. This largely prevents uncontrolled up-regulation of PTH while stimulating FGF23 synthesis. The homeostatic response also prevents the striking suppression of *Cyp24a1* observed in the M1-IKO mice, thereby contributing to the successful preservation of 1,25(OH)$_2$D$_3$. It is possible that the full brunt of the loss of *Cyp27b1* sensitivity to FGF23 and 1,25(OH)$_2$D$_3$ suppression in the M21-IKO mice may be observed only under conditions in which 1,25(OH)$_2$D$_3$ and FGF23 are elevated, and both hypercalcemia and hyperphosphatemia are evident (38). Nevertheless, the current results in M21-IKO mice highlight not only the nature of the exquisite homeostatic circuits that prevail *in vivo* to maintain mineral balance but demonstrate how the levels of key players are also modulated to achieve a normalized calcium and phosphate outcome. The inability of PTH to induce *Cyp27b1* expression in M1-IKO mice almost fully compromises the capacity of *Cyp27b1* and *Cyp24a1* to maintain 1,25(OH)$_2$D$_3$ levels, highlighting the essential role of PTH in the control of skeletal growth and development as well as the maintenance of mineral homeostasis.

The presence of a unique module in the kidney that mediates the regulation of *Cyp27b1* by key hormones involved in mineral homeostasis together with its absence in NRTCs suggests that the primary role of *Cyp27b1* in the kidney is to produce circulating blood levels of 1,25(OH)$_2$D$_3$ that can orchestrate the expression of genes in the intestine, kidney, and bone, which are responsible for global mineral homeostasis. The absence of this

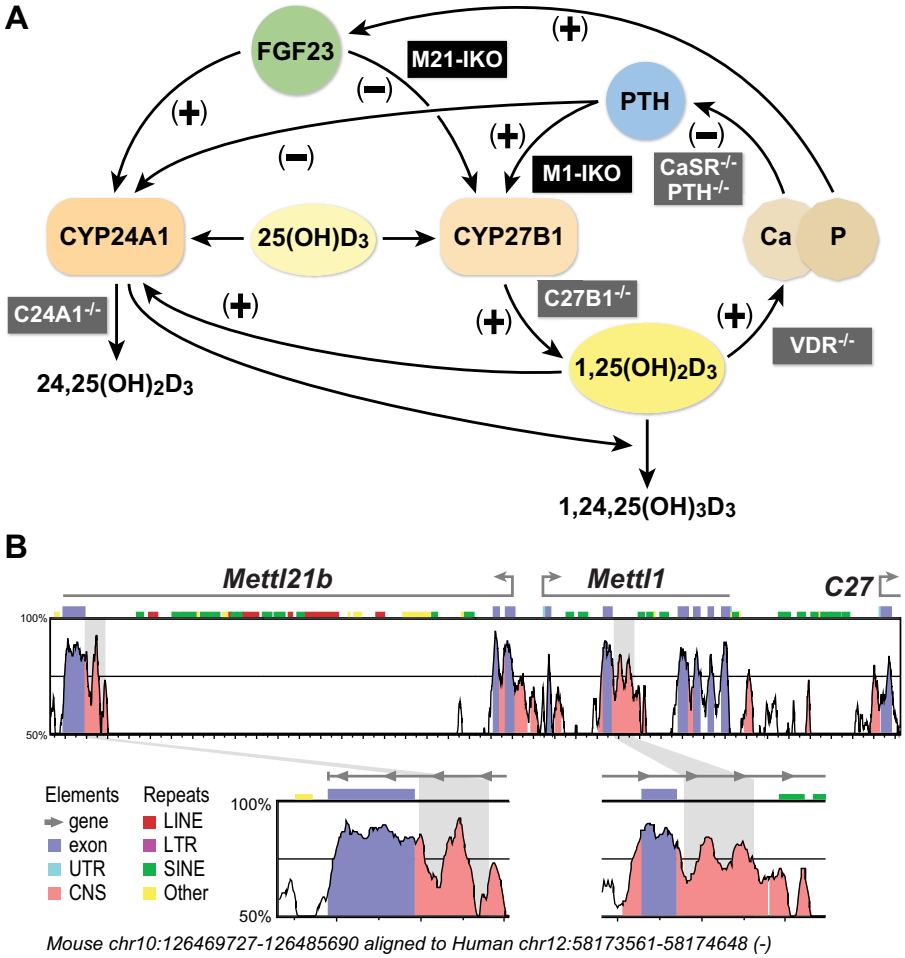

Figure 12. Homeostatic regulation of calcium and phosphate and conservation to human. *A,* schematic diagram for the homeostatic regulation of calcium and phosphate. *B, in silico* VISTA analysis of conservation between mouse and human CYP27B1 genomic loci. Conservation score reaches significance at 75% (indicated by *black middle line*) for exons (*blue*) and M1 and M21 enhancer regions (*coral*, highlighted by *gray boxes*). Other genomic features are as indicated in the figure.

endocrine module in NRTCs and the simultaneous presence of an independent module outside the KS-ERM that controls *Cyp27b1* expression in NRTCs (NRTC-RM) suggests that the expression of *Cyp27b1* in these cell types serves an alternative function to regulate the production of autocrine $1,25(OH)_2D_3$ that controls cell-specific gene activation and local pleiotropic biological activities (46). If these separate roles of *Cyp27b1* in the kidney and NRTCs are correct, it implies the existence of two relatively distinct spheres of vitamin D influence, the first comprising the control of mineral metabolism and the second consisting of the regulation of numerous biological activities that are cell type-specific and independent of mineral metabolism. Most importantly, this thesis indicates that the mechanistic basis for these two biologically active domains of vitamin D action are largely determined by the differential regulation of *Cyp27b1* in these two tissue classes. These two domains are unlikely to be fully independent, however, considering that extracellular calcium and phosphate levels impact all cell types and that endocrine regulation by vitamin D also influences circulating $25(OH)D_3$, the common substrate for *Cyp27b1* activity in both tissue types. Conversely, certain biological actions of vitamin D in NRTCs are also likely to impact the orchestration of mineral homeostasis by the intestine, kidney, and bone as well. For example, the potential impact of vitamin D on insulin secretion, utilization, and energy metabolism is likely to impact the maintenance of mineral homeostasis (47). We argue that the current mouse models we have created, as well as additional models in preparation, will allow us to isolate the activities of each sphere of influence independently, thereby permitting a precise determination of not only the impact of locally produced $1,25(OH)_2D_3$ on the biological activities of NRTCs but of the dependence of these activities on circulating $1,25(OH)_2D_3$ produced by the kidney. This is important because a central clinical issue currently is the impact of vitamin D supplementation on $25(OH)D_3$ levels that are hypothesized to represent a primary determinant of the local production of $1,25(OH)_2D_3$ (48, 49). Of greater importance, however, is the fact that both spheres of vitamin D influence may also be altered in disease, as illustrated in chronic kidney disease (40), autoimmune disease (50), and cancer (51), where both genetic and epigenetic changes could affect both the production and utilization of $1,25(OH)_2D_3$. These possibilities are likely to influence the utility of vitamin D analogues in disease and open the question as to whether tissue-selective modulation of *Cyp27b1* expression may represent an alternative approach to vitamin D therapeutics.

The implications for the locations of regulatory enhancers for the expression of both *Cyp27b1* and *Mettl21b* are significant relative to genome-wide association studies attempting to correlate single nucleotide polymorphisms to the prevalence of autoimmune disease, particularly multiple sclerosis (52–55). In these studies, disease-associated SNPs have been identified in an extended region that contains the *CYP27B1* gene as well as neighboring genes that include *METTL1* and *METTL21B* (*FAM119B*) (56, 57). Indeed, some genotypes appear to be preferential for the altered expression of *CYP27B1*, although observed co-regulation of the *METTL21B* gene has introduced some complexity. Importantly, the human *CYP27B1* locus and adjacent genes on chromosome 12 are syntenic on the reverse strand with the mouse haplotype. In fact, a VISTA analysis of genomic conservation indicates not only that this is the case but that the only non-exonic regions that reach significance are those in which we have identified enhancers (Fig. 12*B*). Our discovery that the regulatory regions that control the mouse *Cyp27b1* gene in the kidney are embedded within the introns of *Mettl1* and *Mettl21b* and that *Mettl21b* is also co-regulated by PTH, FGF23, and $1,25(OH)_2D_3$ are therefore potentially relevant. We hypothesize that the SNPs that have been identified in this region and particularly in the *METTL1* gene in humans may hint at the locations of important regulatory enhancers for both *CYP27B1* and *METTL21B*. It is also of significance that if non-coding SNPs in these genomic regions are linked to the expression of *CYP27B1*, our data would suggest that multiple sclerosis is associated with endocrine production of $1,25(OH)_2D_3$ and not local production by CNS-invasive immune cells. Thus, it will be of interest to determine whether the regulation of the human *CYP27B1* gene in the kidney is modulated through a distal organization similar to that in the mouse and to determine the functional nature of the SNPs that have been identified. In that regard, our studies may have broader implications for vitamin D in other human autoimmune diseases as well.

In summary, a kidney-specific regulatory module has been identified upstream of the *Cyp27b1* gene that controls both the basal and hormone-regulated expression of the gene in the kidney in mice *in vivo*. This module is absent in the *Cyp27b1* region in NRTCs, which accounts for the absence of regulation by PTH, FGF23, and $1,25(OH)_2D_3$ in these cell types. Dissection of this region in mice via CRISPR/Cas9 genome-editing methods has revealed distinct elements responsible for basal expression in the kidney as well as for PTH induction and $1,25(OH)_2D_3$ and FGF23 suppression. The phenotypes of these mouse strains highlight both the genomic and homeostatic circuits that control *Cyp27b1* expression. We conclude that these studies open new avenues to study vitamin D metabolism and its involvement in both mineral metabolism and in other pleiotropic biology *in vivo* in health and disease.

Experimental procedures

Reagents

The following reagents were used for *in vivo* injections: $1\alpha,25(OH)_2D_3$ was obtained from SAFC Global (Madison, WI); PTH(1–84) human, was obtained from Bachem (H-1370.0100 Torrance, CA); mouse FGF23 (2629-FG-025) was from R&D Systems, Minneapolis, MN; and LPS (L6529) was from Sigma.

Antibodies used for ChIP-seq analysis of VDR (C-20, sc-1008, lot no. H1216) were purchased from Santa Cruz Biotechnology, Inc. (Santa Cruz, CA). H3K4me1 (ab8895, lot no. GR283603-1) and H3K36me3 (ab9050, lot no. GR273247-1) were purchased from Abcam (Cambridge, MA). Phosphorylated CREB (Ser-133) (pCREB, 06-519, lot no. 2762242) and H3K9ac (06-942, lot no. 2664263) were purchased from Millipore Corp. (Billerica, MA).

Traditional genotyping PCR was completed with GoTaq (Promega, Madison, WI), and all real-time qPCR was completed with the StepOnePlus using TaqMan for gene expression assays (Applied Biosystems, Foster City, CA). Primers were obtained from IDT (Coralville, IA).

Gene expression

Dissected tissues were frozen immediately in liquid nitrogen and stored at −80 °C. Frozen tissues were homogenized in TRIzol reagent (Life Technologies, Inc.), and RNA was isolated per the manufacturer's instructions. 1 μg of isolated total RNA was DNase-treated, reverse-transcribed using the High Capacity cDNA kit (Applied Biosystems), and then diluted to 100 μl with RNase/DNase free water. qPCR was performed using primers specific to a select set of differentially expressed genes by TaqMan analyses. TaqMan gene expression probes (Applied Biosystems) were used for RT-PCR and are found in Table 1.

ChIP followed by sequencing (ChIP-seq)

ChIP was performed using antibodies listed under "Reagents." ChIP was performed as described previously with several modifications (21). In brief, kidney and TPTG samples were obtained from mice treated with $1,25(OH)_2D_3$, PTH, FGF23, or the corresponding vehicle for 1 h. Two kidneys or 10 TPTGs were combined per replicate, rinsed with ice-cold 1× PBS, and then subjected to immunoprecipitation using either a control IgG or the indicated antibodies. Statistical analysis and data processing for ChIP-seq assays were performed as reported previously (58). The isolated DNA (or input DNA acquired prior to precipitation) was then validated by qPCR and further prepared for ChIP-seq analysis. ChIP-seq libraries were prepared as described previously (58). Conservation analysis was performed with VISTA Point comparing the mouse (mm9) with human (hg19) genomic regions surrounding the *CYP27B1* gene (59).

CRISPR-generated and transgenic mice

The guides used for CRISPR–Cas9-mediated genome editing were optimized for the least number of potential off-target sites and fewest sites within coding exons using the Zhang Laboratory CRISPR Design tool (crispr.mit.edu)[3] and cross-referenced with Liu lab CRISPR-DO (cistrome.org/crispr).[3] The guides (see Table 1) were annealed and cloned into plasmids pX330 or pX458 obtained from Zhang Laboratory via Addgene (Cambridge, MA) as described recently (60). Resulting PCR products were then transcribed *in vitro* utilizing the T7

[3] Please note that the JBC is not responsible for the long-term archiving and maintenance of this site or any other third party hosted site.

Table 1
Primers used for analyses
F is forward, and R is reverse.

Sequence-based reagents	Sequence/source	Ref.
TaqMan primers		
Gapdh	Applied Biosystems	4352339E
Cyp27b1	Applied Biosystems	Mm01165918
Cyp24a1	Applied Biosystems	Mm00487244
Vdr	Applied Biosystems	Mm00437297
Mettl1	Applied Biosystems	Mm00487686
Mettl21b	Applied Biosystems	Mm01165909
Tspan31	Applied Biosystems	Mm00482543
Tsfm	Applied Biosystems	Mm00508436
March9	Applied Biosystems	Mm01165913
Cdk4	Applied Biosystems	Mm00726334
Primers for CRISPR		
M1-IKO Guide 1	GATTAGTTGACCTTTCCTCCTGG	This paper
M1-IKO Guide 2	CAGGAACTCCAGACCATGAGAGG	This paper
M21-IKO Guide 1	CCTACCTTCCCGCTACTGTTGGG	This paper
M21-IKO Guide 2	CCCTTCCTTAGGGACTTCATGGG	This paper
Primers for genotyping		
C27KO KO-F	ACTTTTCTGATTCAGGGATGAAGGTTTAGC	This paper
C27KO KO-R	GAAGGAGGGCAGATTAGATATTCTAGGATGC	This paper
C27KO WT-F	CTCCTGCCAGAGTCTATCCCTG	This paper
C27KO WT-R	GAAGGAGGGCAGATTAGATATTCTAGGATGC	This paper
M1-IKO spanF	AGTGGAGTTTGCAGACATAGGCT	This paper
M1-IKO spanR	TTACCTGTCTATAGGGAAGATG	This paper
M1-IKO internalF	TCTACTCTGGGTCTGTGGCCTT	This paper
M1-IKO internalR	AGCTAGACAGAACAACCGGGG	This paper
M21-IKO spanF	TTCCTCCACTGAGACAAGAGTTA	This paper
M21-IKO spanR	CCTTGCTACTTTCCAACAGCCTGCCT	This paper
M21-IKO internalF	ATGTATCCTCTCCCTCCTGAACA	This paper
M21-IKO internalR	CCCCATACAATAGGGTTTCTCTCTG	This paper

MEGAshortscript kit (Life Technologies, Inc.) (61). The mixture of 50 ng/μl of the produced RNA guides and 40 ng/μl Cas9 protein in injection buffer (5 mM Trizma base, 5 mM Tris-HCl, 0.1 mM EDTA, pH 7.4) was injected into the pronucleus of 1 day-fertilized embryos isolated from hyper-ovulating female C57BL/6 mice, as described previously (62), and implanted into recipient females at the University of Wisconsin-Madison Biotechnology Center Transgenic Animal Facility. The resultant pups were genotyped with spanning primers (Table 1), cloned, and sequenced. The top 10 predicted potential off-target sites were examined by PCR and sequencing analysis.

The VDR-null (VDRKO) strain was produced by targeted ablation of the second zinc finger of the VDR DNA-binding domain (25). VDRKO mice were fed a standard rodent chow diet (5008; Lab Diet, St. Louis, MO). Cyp27b1 null (C27KO) mice were produced by GenOway (Strasbourg, France) with a strategy similar to that previously described (63). In brief, the mouse *Cyp27b1* gene was amplified by PCR using genomic DNA from C57BL/6 ES cells as a template and cloned into the pCR4-TPOP vector (Invitrogen) to create a targeting vector. Two *lox*P sites were inserted in intron 6 and downstream of exon 9 and a positive selection marker, neomycin resistance gene, which is flanked by FRT sites, was introduced between exon 9 and downstream *lox*P site. Diphtheria toxin A was also introduced upstream of the *Cyp27b1* gene as a negative selection marker to reduce the isolation of non-homologous recombined ES cell clones and to enhance the chance to isolate ES cell clones containing the distal *lox*P site. The targeting vector was linearized and electroporated into ES cells. The recombined ES cell clones identified by the selection, PCR confirmation, and Southern blot analysis were then injected into C57BL/6 blastocysts to create chimeric mice, and the injected blastocysts were reimplanted into OF1 pseudopregnant females and allowed to develop. To remove the selection marker flanked by FRT sites and exons 7–9 of the *Cyp27b1* gene flanked by *lox*P sites, the recombinant mice were sequentially bred with Flp-recombinase expressing deleter mice and then Cre-recombinase expressing deleter mice. For genotyping, a primer set amplifying a DNA region between the last exon and downstream of the last exon (880 bp) and a primer set amplifying a DNA region between intron 5 and downstream of the last exon (560 bp) were used for WT and the deleted alleles, respectively (Table 1).

Animal studies

Genetically modified mice were outbred with C57BL/6 mice (Envigo, Indianapolis, IN, and The Jackson Laboratory, Bar Harbor, ME) as heterozygotes. Mice were housed in high-density ventilated caging in the Animal Research Facility of the University of Wisconsin-Madison under 12-h light/dark cycles, 72 °F temperature, and 45% humidity. All mice used in this study were maintained on a standard rodent chow diet (5008, Lab Diet, St. Louis, MO), aged 8–9 weeks, and backcrossed five or more generations with WT mice unless otherwise indicated. For the $1,25(OH)_2D_3$ rescue diet study, 3-week-old mice were fed either a $1,25(OH)_2D_3$ rescue diet (5008 chow diet + 1 ng/g $1,25(OH)_2D_3$) or standard chow (5008) for 5 weeks, at which time the animals were sacrificed, and tissues were collected. For the vitamin D_3-deficiency study, 3-week-old mice were fed either a vitamin D_3-deficient diet containing 0.6% calcium and 0.4% phosphorus (TD.01102, Envigo, Madison, WI) or a control diet containing 0.6% calcium, 0.4% phosphorus, and 2200 IU vitamin D/kg (TD.97191, Envigo) for 5 weeks, at which time animals were sacrificed, and tissues were collected. All experiments and tissue collections were performed in the

procedure rooms in the Research Animal Facility of the University of Wisconsin-Madison. All animal studies were reviewed and approved by the Research Animal Care and Use Committee of the University of Wisconsin-Madison (A005478).

Animals were injected intraperitoneally with 10 ng/g body weight (bw) $1,25(OH)_2D_3$ (in propylene glycol), 230 ng/g bw PTH(1–84) (in PBS), 50 ng/g bw FGF23 (in PBS + 0.1% BSA), 10 mg/kg bw LPS (in PBS), or vehicle (EtOH or PBS). Animals were sacrificed, and tissues were collected 1 h after PTH injection, 3 h after FGF23 injection, and 6 h after $1,25(OH)_2D_3$ and LPS injections. Unless otherwise indicated, all experiments were done with equal numbers of males and females ($n \geq 6$). There were no differences in our data between males and females; therefore, the data presented combine both males and females in all studies unless otherwise indicated.

Western blot analysis

Mitochondrial extracts from whole kidneys were prepared with a Potter-Elvehjem homogenization tube using 5 ml of homogenization buffer (250 mM sucrose, 19 mM HEPES, 10 mM KCl, pH 7.4, plus protease inhibitor mixture (Roche Applied Science)). The resulting homogenate was centrifuged (4000 × *g*) for 1 min (4 °C). The supernatant was centrifuged (9000 × *g*) for 20 min (4 °C), and the resulting pellet was resuspended in 1 ml of homogenization buffer and centrifuged (9000 × *g*) for 10 min (4 °C). The pellet was solubilized in 500 μl of SDS loading buffer (100 mM Tris-HCl, pH 6.8, 4% SDS, 0.2% bromphenol blue, 20% glycerol, 200 mM DTT). 30 μl of sample was heated to 95 °C for 5 min and subjected to 12% SDS-PAGE. The kidney mitochondrial extracts were subjected to Western blot analysis as described previously (58) using primary antibodies to CYP27B1 (G-20, sc-49644, Santa Cruz Biotechnology, Inc., lot no. B1114, 1:500) and VDAC/Porin (ab15895, Abcam, lot no. GR264581-2, 1:5000) followed by secondary antibodies donkey α-goat IgG-HRP (sc-2020, Santa Cruz Biotechnology, Inc., 1:2000) and goat α-rabbit IgG-HRP (sc-2004, Santa Cruz Biotechnology, Inc., 1:5000), respectively.

Whole-kidney tissue lysates were prepared using Tissue Lysis Buffer (10 mM Tris-Cl, pH 8, 300 mM KCl, 1 mM EDTA, 2 mM DTT, and protease inhibitor mixture), and protein concentrations were measured using protein assay (Bio-Rad). 80 μg of lysates were denatured and subjected to 12% SDS-PAGE. Subsequently, whole-kidney lysates were subjected to Western blot analysis, as described previously (58), using primary antibodies to VDR (9A7 (64), 1:2000) and β-tubulin (H-235, sc-9104, Santa Cruz Biotechnology, Inc.; lot no. E0913, 1:5000) followed by secondary antibodies goat α-rat IgG-HRP (sc-2032, Santa Cruz Biotechnology, Inc., 1:2000) and goat α-rabbit IgG-HRP (1:5000), respectively. Because of the overlapping molecular weights of VDR and β-tubulin, 1 aliquot of sample was run over two gels and immunoblotted as described above.

Blood chemistry

Cardiac blood was collected at the time of sacrifice. Collected blood was split into serum- or EDTA-treated plasma, incubated at room temperature for 30 min, followed by centrifugation at 6000 rpm for 12 min (twice) to obtain serum or EDTA plasma. Serum calcium and phosphate levels were measured using QuantiChrom™ calcium assay kit (DICA-500, BioAssay Systems, Hayward, CA) and QuantiChrom™ phosphate assay kit (DIPI-500, BioAssay Systems). Circulating intact FGF23 and PTH were measured in EDTA plasma via mouse/rat FGF-23 (intact) ELISA kit (60-6800, Immutopics, San Clemente, CA) and mouse PTH(1–84) ELISA kit (60-2305, Immutopics), respectively.

Quantification of serum vitamin D metabolites

Serum $25(OH)D_3$, $25(OH)D_3$-26,23-lactone, and $24,25(OH)_2D_3$ were quantified by LC-MS/MS, using previously published methods (14, 65), except that the starting volume of serum was reduced to 25 μl and diluted with 275 μl of water after addition of internal standard where an equivalent of 19 μl of serum was analyzed per injection. Vitamin D metabolite levels were determined in individual animals. Concentration of $25(OH)D_3$-26,23-lactone was estimated using the calibration line for $24,25(OH)_2D_3$ and recovery of d_6-$24,25(OH)_2D_3$. We observed that simultaneous assay of $1,25(OH)_2D_3$ and $1,24,25(OH)_3D_3$ was possible based on cross-reactivity of an anti-$1,25(OH)_2D_3$ antibody slurry (Immundiagnostik) with $1,24,25(OH)_3D_3$. A six-point calibrator for $1,25\text{-}(OH)_2D_3$ and $1,24,25(OH)_3D_3$ was created in vitamin D-stripped serum (MSG2000; Golden West Biologicals), containing 5–300 pg/ml $1,25(OH)_2D_3$ (Cerilliant) and 1–25 pg/ml $1,24,25(OH)_3D_3$. 150-μl aliquots of serum were equilibrated with 200 pg/ml d_6-$1,25(OH)_2D_3$ and 12.5 pg/ml d_6-$1,24,25(OH)_3D_3$, which were generated in-house by HPLC purification from a CYP24A1 expression system incubated with d_6-$1,25(OH)_2D_3$ based on previously described methodology (66). The serum was incubated with 100 μl of anti-$1,25(OH)_2D_3$ antibody slurry (67) for 2 h at room temperature with orbital shaking at 1200 rpm. The slurry was isolated by vacuum filtration and rinsed four times with 400-μl aliquots of water, and vitamin D metabolites were eluted two times with 400 μl of ethanol. The ethanol eluate was evaporated to dryness and derivatized with 4-[2-(3,4-dihydro-6,7-dimethoxy-4-methyl-3-oxo-2-quinoxalinyl)ethyl]-3*H*-1,2,4-triazole-3.5-(4*H*)-dione (DMEQ-TAD) as described previously. The sample was re-dissolved in 50 μl of mobile phase consisting of 50:50 (% by volume) methanol/water, and 35 μl (110-μl eq of serum) was injected into the LC-MS/MS system as described previously (68). Multiple reaction monitoring transitions used for analysis of $1,25\text{-}(OH)_2D_3$ and $1,24,25(OH)_3D_3$ were as follows: m/z $762 \rightarrow 468 + 762 \rightarrow 484$ and $778 \rightarrow 468 + 778 \rightarrow 484$, respectively.

BMD and μCT analysis

At 8–9 weeks of age, BMDs of the CRISPR-generated mice and their WT littermates were measured and analyzed by dual X-ray absorptiometry with a PIXImus densitometer (GE-Lunar Corp., Madison, WI), as described previously (63). μCT analyses were performed using a high-resolution benchtop Scanco uCT50 (Scanco Medical, Bassersdorf, Switzerland) at the Vanderbilt Center for Bone Biology. Tomographic images were acquired at 70 peak kilovoltages and 200 μA with an isotropic voxel size of 12.0 mm and at an integration time of 400 ms with 1000 projections per 360° rotation. Reconstructed μCT images

were binarized, using a Gaussian noise filter with $\sigma = 0.3$ and support = 1 and a threshold of 470 mg of hydroxyapatite/ccm for trabecular bone or 0.3, 1, and 733 mg of HA/cm^3 for midshaft cortical bone. The volume of interest for trabecular bone in the distal femoral metaphysis was the entire medullary area located 0.360–1.560 mm proximal to the distal growth plate. The midshaft volume of interest was a 1.2-mm-long segment of cortical bone centered between the femoral head and surface of the distal condyles. All volumetric structural parameters were calculated from the 3D renderings using Scanco Evaluation software following standard methods and nomenclature (69).

Immunohistochemistry

Mice were perfused with PBS followed by 4% paraformaldehyde. The collected tissues were immersed overnight in 4% paraformaldehyde and then overnight again in 30% sucrose. Thyroparathyroid tissues were processed to prepare frozen tissue blocks using Neg-50 (Richard-Allan Scientific) and cut into 10-μm sections with an HM5050E microtome (Microm). The tissue sections were stained with hematoxylin stain solution (3530-32; Ricca Chemical Co.) and eosin-Y (Fisher). The stained tissue sections were mounted with Permount (Fisher). Images for histological assay were taken using an ECLIPSE Ti-S microscope (Nikon) and QICAM 12-bit Mono Fast 1394 cooled camera (QImaging). PTG sizes were determined using ImageJ software. After μCT analysis, undecalcified tibiae were embedded in methyl methacrylate, sectioned on an automatic retractable Microtom 355 with a D-profile, tungsten carbide steel knife at 4 μm. Adjacent sections were stained with Masson trichrome (70) or with von Kossa to visualize mineralized bone.

T cell activation

Spleen CD4$^+$ or CD8$^+$ T cells were isolated by negative selection using EasySep mouse CD4$^+$ or CD8$^+$ T cell isolation kit (Stemcell Technologies, Vancouver, British Columbia, Canada) per the manufacturer's instructions. Isolated CD4$^+$ or CD8$^+$ T cells were plated in 24-well plates with a density of 1×10^6 cells/well and treated 3 h with vehicle (PBS) or 25 μl/well of CD3/CD28 mouse T-activator Dynabeads (Gibco, Life Technologies, Inc.). In addition, isolated CD4$^+$ or CD8$^+$ T cells were plated in 24-well plates with a density of 1×10^6 cells/well and treated 3 h with vehicle (EtOH) or 100 nM 1,25(OH)$_2$D$_3$.

Statistical evaluation

Data were analyzed using GraphPad Prism 7 software (GraphPad Software, Inc., La Jolla, CA) and in consultation with the Statistics Department, University of Wisconsin. All values are reported as the means ± S.E., and differences between group means were evaluated using one-way ANOVA, two-way ANOVA, or Student's *t* test as indicated in the figure legends.

Author contributions—M. B. M. and J. W. P. conceived the paper; M. B. M., N. A. B., M. O., S. M. L., and M. K. performed the investigation; M. B. M. and J. W. P. wrote the original draft; N. A. B., M. K., and G. J. reviewed and edited the paper, M. B. M. performed data curation.

Acknowledgments—We thank Dr. Dan Perrien at the Vanderbilt Center for Bone Biology for μCT analysis and growth plate slide preparation. We thank the University of Wisconsin Biotechnology Center Transgenic Animal Facility for generating the CRISPR/Cas9 enhancer-deleted mice. We also thank Professor Mark R. Haussler for historical perspective and careful reading of the manuscript. Through a Queen's University/Waters Corp. agreement, Waters generously provided the LC-MS/MS instrumentation used in this study.

References

1. DeLuca, H. F. (2004) Overview of general physiologic features and functions of vitamin D. *Am. J. Clin. Nutr.* **80,** 1689S-1696S
2. Jones, G., Prosser, D. E., and Kaufmann, M. (2014) Cytochrome P450-mediated metabolism of vitamin D. *J. Lipid Res.* **55,** 13–31
3. Jones, G., Prosser, D. E., and Kaufmann, M. (2012) 25-Hydroxyvitamin D-24-hydroxylase (CYP24A1): its important role in the degradation of vitamin D. *Arch. Biochem. Biophys.* **523,** 9–18
4. Adams, J. S., and Hewison, M. (2012) Extrarenal expression of the 25-hydroxyvitamin D-1-hydroxylase. *Arch. Biochem. Biophys.* **523,** 95–102
5. Bikle, D. D. (2011) Vitamin D metabolism and function in the skin. *Mol. Cell. Endocrinol.* **347,** 80–89
6. DeLuca, H. F. (1972) Parathyroid hormone as a trophic hormone for 1,25-dihydroxyvitamin D3, the metabolically active form of vitamin D. *N. Engl. J. Med.* **287,** 250–251
7. Garabedian, M., Holick, M. F., Deluca, H. F., and Boyle, I. T. (1972) Control of 25-hydroxycholecalciferol metabolism by parathyroid glands. *Proc. Natl. Acad. Sci. U.S.A.* **69,** 1673–1676
8. Tanaka, Y., and DeLuca, H. (1984) Rat renal 25-hydroxyvitamin D3 1- and 24-hydroxylases: their *in vivo* regulation. *Am. J. Physiol.* **246,** E168–E173
9. Shimada, T., Hasegawa, H., Yamazaki, Y., Muto, T., Hino, R., Takeuchi, Y., Fujita, T., Nakahara, K., Fukumoto, S., and Yamashita, T. (2004) FGF-23 is a potent regulator of vitamin D metabolism and phosphate homeostasis. *J. Bone Miner. Res.* **19,** 429–435
10. Shimada, T., Kakitani, M., Yamazaki, Y., Hasegawa, H., Takeuchi, Y., Fujita, T., Fukumoto, S., Tomizuka, K., and Yamashita, T. (2004) Targeted ablation of Fgf23 demonstrates an essential physiological role of FGF23 in phosphate and vitamin D metabolism. *J. Clin. Invest.* **113,** 561–568
11. Chandler, J. S., Chandler, S. K., Pike, J. W., and Haussler, M. R. (1984) 1,25-Dihydroxyvitamin D3 induces 25-hydroxyvitamin D3–24-hydroxylase in a cultured monkey kidney cell line (LLC-MK2) apparently deficient in the high affinity receptor for the hormone. *J. Biol. Chem.* **259,** 2214–2222
12. Zierold, C., Darwish, H. M., and DeLuca, H. F. (1995) Two vitamin D response elements function in the rat 1,25-dihydroxyvitamin D24-hydroxylase promoter. *J. Biol. Chem.* **270,** 1675–1678
13. Quarles, L. D. (2012) Skeletal secretion of FGF-23 regulates phosphate and vitamin D metabolism. *Nat. Rev. Endocrinol.* **8,** 276–286
14. Kaufmann, M., Lee, S. M., Pike, J. W., and Jones, G. (2015) A high-calcium and phosphate rescue diet and VDR-expressing transgenes normalize serum vitamin D metabolite profiles and renal Cyp27b1 and Cyp24a1 expression in VDR null mice. *Endocrinology* **156,** 4388–4397
15. Armbrecht, H. J., Hodam, T. L., and Boltz, M. A. (2003) Hormonal regulation of 25-hydroxyvitamin D3–1α-hydroxylase and 24-hydroxylase gene transcription in opossum kidney cells. *Arch. Biochem. Biophys.* **409,** 298–304
16. Pike, J. W., Meyer, M. B., Benkusky, N. A., Lee, S. M., St John, H., Carlson, A., Onal, M., and Shamsuzzaman, S. (2016) Genomic determinants of vitamin D-regulated gene expression. *Vitam. Horm.* **100,** 21–44
17. Farrow, E. G., Davis, S. I., Summers, L. J., and White, K. E. (2009) Initial FGF23-mediated signaling occurs in the distal convoluted tubule. *J. Am. Soc. Nephrol.* **20,** 955–960
18. Portale, A. A., Zhang, M. Y., David, V., Martin, A., Jiao, Y., Gu, W., and Perwad, F. (2015) Characterization of FGF23-dependent Egr-1 cistrome in the mouse renal proximal tubule. *PLoS ONE* **10,** e0142924

19. Meyer, M. B., Benkusky, N. A., Sen, B., Rubin, J., and Pike, J. W. (2016) Epigenetic plasticity drives adipogenic and osteogenic differentiation of marrow-derived mesenchymal stem cells. *J. Biol. Chem.* **291,** 17829–17847
20. Pike, J. W., and Meyer, M. B. (2012) Regulation of mouse Cyp24a1 expression via promoter-proximal and downstream-distal enhancers highlights new concepts of 1,25-dihydroxyvitamin D(3) action. *Arch. Biochem. Biophys.* **523,** 2–8
21. Meyer, M. B., Zella, L. A., Nerenz, R. D., and Pike, J. W. (2007) Characterizing early events associated with the activation of target genes by 1,25-dihydroxyvitamin D_3 in mouse kidney and intestine *in vivo*. *J. Biol. Chem.* **282,** 22344–22352
22. Cartlidge, R. A., Knebel, A., Peggie, M., Alexandrov, A., Phizicky, E. M., and Cohen, P. (2005) The tRNA methylase METTL1 is phosphorylated and inactivated by PKB and RSK *in vitro* and in cells. *EMBO J.* **24,** 1696–1705
23. Malecki, J., Aileni, V. K., Ho, A. Y. Y., Schwarz, J., Moen, A., Sørensen, V., Nilges, B. S., Jakobsson, M. E., Leidel, S. A., and Falnes, P. (2017) The novel lysine specific methyltransferase METTL21B affects mRNA translation through inducible and dynamic methylation of Lys-165 in human eukaryotic elongation factor 1α (eEF1A). *Nucleic Acids Res.* **45,** 4370–4389
24. Ernst, J., Kheradpour, P., Mikkelsen, T. S., Shoresh, N., Ward, L. D., Epstein, C. B., Zhang, X., Wang, L., Issner, R., Coyne, M., Ku, M., Durham, T., Kellis, M., and Bernstein, B. E. (2011) Mapping and analysis of chromatin state dynamics in nine human cell types. *Nature* **473,** 43–49
25. Li, Y. C., Pirro, A. E., Amling, M., Delling, G., Baron, R., Bronson, R., and Demay, M. B. (1997) Targeted ablation of the vitamin D receptor: an animal model of vitamin D-dependent rickets type II with alopecia. *Proc. Natl. Acad. Sci. U.S.A.* **94,** 9831–9835
26. Dardenne, O., Prud'homme, J., Arabian, A., Glorieux, F. H., and St-Arnaud, R. (2001) Targeted inactivation of the 25-hydroxyvitamin D(3)-1(α)-hydroxylase gene (CYP27B1) creates an animal model of pseudovitamin D-deficiency rickets. *Endocrinology* **142,** 3135–3141
27. Mouse ENCODE Consortium, Stamatoyannopoulos, J. A., Snyder, M., Hardison, R., Ren, B., Gingeras, T., Gilbert, D. M., Groudine, M., Bender, M., Kaul, R., Canfield, T., Giste, E., Johnson, A., Zhang, M., Balasundaram, G., *et al.* (2012) An encyclopedia of mouse DNA elements (Mouse ENCODE). *Genome Biol.* **13,** 418
28. Liu, F. (2017) Enhancer-derived RNA: a primer. *Genomics Proteomics Bioinformatics* **15,** 196–200
29. Ong, C. T., and Corces, V. G. (2014) CTCF: an architectural protein bridging genome topology and function. *Nat. Rev. Genet.* **15,** 234–246
30. Nichols, M. H., and Corces, V. G. (2015) A CTCF Code for 3D genome architecture. *Cell* **162,** 703–705
31. Nora, E. P., Goloborodko, A., Valton, A. L., Gibcus, J. H., Uebersohn, A., Abdennur, N., Dekker, J., Mirny, L. A., and Bruneau, B. G. (2017) Targeted degradation of CTCF decouples local insulation of chromosome domains from genomic compartmentalization. *Cell* **169,** 930–944
32. Cong, L., Ran, F. A., Cox, D., Lin, S., Barretto, R., Habib, N., Hsu, P. D., Wu, X., Jiang, W., Marraffini, L. A., and Zhang, F. (2013) Multiplex genome engineering using CRISPR/Cas systems. *Science* **339,** 819–823
33. Nguyen-Yamamoto, L., Karaplis, A. C., St-Arnaud, R., and Goltzman, D. (2017) Fibroblast growth factor 23 regulation by systemic and local osteoblast-synthesized 1,25-dihydroxyvitamin D. *J. Am. Soc. Nephrol.* **28,** 586–597
34. Healy, K. D., Zella, J. B., Prahl, J. M., and DeLuca, H. F. (2003) Regulation of the murine renal vitamin D receptor by 1,25-dihydroxyvitamin D3 and calcium. *Proc. Natl. Acad. Sci. U.S.A.* **100,** 9733–9737
35. Chandler, J. S., Pike, J. W., and Haussler, M. R. (1982) Biosynthesis, purification and receptor binding properties of high specific radioactivity 1α, 24(R),25-trihydroxy-[26,27-methyl-3H]-vitamin D3. *J. Steroid Biochem.* **16,** 303–310
36. Thomasset, M., Cuisinier-Gleizes, P., Mathieu, H., and DeLuca, H. F. (1980) Intestinal calcium-binding protein (CaBP) and bone calcium mobilization in response to 1,24(R),25-(OH)3D3. Comparative effects of 1,25-(OH)2D3 and 24(R),25-(OH)2D3 in rats. *Mol. Pharmacol.* **17,** 362–366
37. Liu, S., Tang, W., Zhou, J., Stubbs, J. R., Luo, Q., Pi, M., and Quarles, L. D. (2006) Fibroblast growth factor 23 is a counter-regulatory phosphaturic hormone for vitamin D. *J. Am. Soc. Nephrol.* **17,** 1305–1315
38. Haussler, M. R., Whitfield, G. K., Haussler, C. A., Sabir, M. S., Khan, Z., Sandoval, R., and Jurutka, P. W. (2016) 1,25-Dihydroxyvitamin D and Klotho: a tale of two renal hormones coming of age. *Vitam. Horm.* **100,** 165–230
39. Chow, E. C., Quach, H. P., Vieth, R., and Pang, K. S. (2013) Temporal changes in tissue 1α,25-dihydroxyvitamin D3, vitamin D receptor target genes, and calcium and PTH levels after 1,25(OH)2D3 treatment in mice. *Am. J. Physiol. Endocrinol. Metab.* **304,** E977–E989
40. Quarles, L. D. (2012) Role of FGF23 in vitamin D and phosphate metabolism: implications in chronic kidney disease. *Exp. Cell Res.* **318,** 1040–1048
41. Hewison, M. (2011) Vitamin D and innate and adaptive immunity. *Vitam. Horm.* **86,** 23–62
42. Adams, J. S., Rafison, B., Witzel, S., Reyes, R. E., Shieh, A., Chun, R., Zavala, K., Hewison, M., and Liu, P. T. (2014) Regulation of the extrarenal CYP27B1-hydroxylase. *J. Steroid Biochem. Mol. Biol.* **144,** 22–27
43. Ritter, C. S., Haughey, B. H., Armbrecht, H. J., and Brown, A. J. (2012) Distribution and regulation of the 25-hydroxyvitamin D3 1α-hydroxylase in human parathyroid glands. *J. Steroid. Biochem. Mol. Biol.* **130,** 73–80
44. Segersten, U., Correa, P., Hewison, M., Hellman, P., Dralle, H., Carling, T., Akerström, G., and Westin, G. (2002) 25-hydroxyvitamin D(3)-1α-hydroxylase expression in normal and pathological parathyroid glands. *J. Clin. Endocrinol. Metab.* **87,** 2967–2972
45. Meir, T., Levi, R., Lieben, L., Libutti, S., Carmeliet, G., Bouillon, R., Silver, J., and Naveh-Many, T. (2009) Deletion of the vitamin D receptor specifically in the parathyroid demonstrates a limited role for the receptor in parathyroid physiology. *Am. J. Physiol. Renal. Physiol.* **297,** F1192–F1198
46. Hewison, M., Burke, F., Evans, K. N., Lammas, D. A., Sansom, D. M., Liu, P., Modlin, R. L., and Adams, J. S. (2007) Extra-renal 25-hydroxyvitamin D3–1α-hydroxylase in human health and disease. *J. Steroid. Biochem. Mol. Biol.* **103,** 316–321
47. Bouillon, R., Carmeliet, G., Lieben, L., Watanabe, M., Perino, A., Auwerx, J., Schoonjans, K., and Verstuyf, A. (2014) Vitamin D and energy homeostasis– of mice and men. *Nat. Rev. Endocrinol.* **10,** 79–87
48. Bouillon, R. (2017) Comparative analysis of nutritional guidelines for vitamin D. *Nat. Rev. Endocrinol.* **13,** 466–479
49. Bouillon, R. (2017) Optimal vitamin D supplementation strategies. *Endocrine* **56,** 225–226
50. Cantorna, M. T., Hayes, C. E., and DeLuca, H. F. (1996) 1,25-Dihydroxyvitamin D3 reversibly blocks the progression of relapsing encephalomyelitis, a model of multiple sclerosis. *Proc. Natl. Acad. Sci. U.S.A.* **93,** 7861–7864
51. Feldman, D., Krishnan, A. V., Swami, S., Giovannucci, E., and Feldman, B. J. (2014) The role of vitamin D in reducing cancer risk and progression. *Nat. Rev. Cancer* **14,** 342–357
52. International Multiple Sclerosis Genetics Consortium, Wellcome Trust Case Control Consortium 2, Sawcer, S., Hellenthal, G., Pirinen, M., Spencer, C. C., Patsopoulos, N. A., Moutsianas, L., Dilthey, A., Su, Z., Freeman, C., Hunt, S. E., Edkins, S., Gray, E., Booth, D. R., *et al.* (2011) Genetic risk and a primary role for cell-mediated immune mechanisms in multiple sclerosis. *Nature* **476,** 214–219
53. Raychaudhuri, S., Remmers, E. F., Lee, A. T., Hackett, R., Guiducci, C., Burtt, N. P., Gianniny, L., Korman, B. D., Padyukov, L., Kurreeman, F. A., Chang, M., Catanese, J. J., Ding, B., Wong, S., van der Helm-van Mil, A. H., *et al.* (2008) Common variants at CD40 and other loci confer risk of rheumatoid arthritis. *Nat. Genet.* **40,** 1216–1223
54. Ramagopalan, S. V., Dyment, D. A., Cader, M. Z., Morrison, K. M., Disanto, G., Morahan, J. M., Berlanga-Taylor, A. J., Handel, A., De Luca, G. C., Sadovnick, A. D., Lepage, P., Montpetit, A., and Ebers, G. C. (2011) Rare variants in the CYP27B1 gene are associated with multiple sclerosis. *Ann. Neurol.* **70,** 881–886
55. Sundqvist, E., Bäärnhielm, M., Alfredsson, L., Hillert, J., Olsson, T., and Kockum, I. (2010) Confirmation of association between multiple sclerosis and CYP27B1. *Eur. J. Hum. Genet.* **18,** 1349–1352
56. Alcina, A., Fedetz, M., Fernández, O., Saiz, A., Izquierdo, G., Lucas, M., Leyva, L., García-León, J. A., Abad-Grau Mdel, M., Alloza, I., Antigüedad,

A., Garcia-Barcina, M. J., Vandenbroeck, K., Varadé, J., de la Hera, B., *et al.* (2013) Identification of a functional variant in the KIF5A-CYP27B1-METTL1-FAM119B locus associated with multiple sclerosis. *J. Med. Genet.* **50,** 25–33

57. Karaky, M., Alcina, A., Fedetz, M., Barrionuevo, C., Potenciano, V., Delgado, C., Izquierdo, G., and Matesanz, F. (2016) The multiple sclerosis-associated regulatory variant rs10877013 affects expression of CYP27B1 and VDR under inflammatory or vitamin D stimuli. *Mult. Scler.* **22,** 999–1006
58. Meyer, M. B., Benkusky, N. A., and Pike, J. W. (2014) The RUNX2 cistrome in osteoblasts: characterization, down-regulation following differentiation, and relationship to gene expression. *J. Biol. Chem.* **289,** 16016–16031
59. Frazer, K. A., Pachter, L., Poliakov, A., Rubin, E. M., and Dubchak, I. (2004) VISTA: computational tools for comparative genomics. *Nucleic Acids Res.* **32,** W273–W279
60. Meyer, M. B., Benkusky, N. A., Onal, M., and Pike, J. W. (2016) Selective regulation of *Mmp13* by $1,25(OH)_2D_3$, PTH, and Osterix through distal enhancers. *J. Steroid Biochem. Mol. Biol.* **164,** 258–264
61. Wang, H., Yang, H., Shivalila, C. S., Dawlaty, M. M., Cheng, A. W., Zhang, F., and Jaenisch, R. (2013) One-step generation of mice carrying mutations in multiple genes by CRISPR/Cas-mediated genome engineering. *Cell* **153,** 910–918
62. Meyer, M., de Angelis, M. H., Wurst, W., and Kühn, R. (2010) Gene targeting by homologous recombination in mouse zygotes mediated by zinc-finger nucleases. *Proc. Natl. Acad. Sci. U.S.A.* **107,** 15022–15026
63. Onal, M., St John, H. C., Danielson, A. L., and Pike, J. W. (2016) Deletion of the distal Tnfsf11 RL-D2 enhancer that contributes to PTH-mediated RANKL expression in osteoblast lineage cells results in a high bone mass phenotype in mice. *J. Bone Miner. Res.* **31,** 416–429
64. Pike, J. W., Donaldson, C. A., Marion, S. L., and Haussler, M. R. (1982) Development of hybridomas secreting monoclonal antibodies to the chicken intestinal 1 α,25-dihydroxyvitamin D3 receptor. *Proc. Natl. Acad. Sci. U.S.A.* **79,** 7719–7723
65. Kaufmann, M., Gallagher, J. C., Peacock, M., Schlingmann, K. P., Konrad, M., DeLuca, H. F., Sigueiro, R., Lopez, B., Mourino, A., Maestro, M., St-Arnaud, R., Finkelstein, J. S., Cooper, D. P., and Jones, G. (2014) Clinical utility of simultaneous quantitation of 25-hydroxyvitamin D and 24,25-dihydroxyvitamin D by LC-MS/MS involving derivatization with DMEQ-TAD. *J. Clin. Endocrinol. Metab.* **99,** 2567–2574
66. Kaufmann, M., Prosser, D. E., and Jones, G. (2011) Bioengineering anabolic vitamin D-25-hydroxylase activity into the human vitamin D catabolic enzyme, cytochrome P450 CYP24A1, by a V391L mutation. *J. Biol. Chem.* **286,** 28729–28737
67. Laha, T. J., Strathmann, F. G., Wang, Z., de Boer, I. H., Thummel, K. E., and Hoofnagle, A. N. (2012) Characterizing antibody cross-reactivity for immunoaffinity purification of analytes prior to multiplexed liquid chromatography-tandem mass spectrometry. *Clin. Chem.* **58,** 1711–1716
68. Kaufmann, M., Morse, N., Molloy, B. J., Cooper, D. P., Schlingmann, K. P., Molin, A., Kottler, M. L., Gallagher, J. C., Armas, L., and Jones, G. (2017) Improved screening test for idiopathic infantile hypercalcemia confirms residual levels of serum 24,25-(OH)2D3 in affected patients. *J. Bone Miner. Res.* **32,** 1589–1596
69. Bouxsein, M. L., Boyd, S. K., Christiansen, B. A., Guldberg, R. E., Jepsen, K. J., and Müller, R. (2010) Guidelines for assessment of bone microstructure in rodents using micro-computed tomography. *J. Bone Miner. Res.* **25,** 1468–1486
70. Perrien, D. S., Akel, N. S., Edwards, P. K., Carver, A. A., Bendre, M. S., Swain, F. L., Skinner, R. A., Hogue, W. R., Nicks, K. M., Pierson, T. M., Suva, L. J., and Gaddy, D. (2007) Inhibin A is an endocrine stimulator of bone mass and strength. *Endocrinology* **148,** 1654–1665